UNIVERSITY OF OKLAHOMA

GRADUATE COLLEGE

EXPLORING IMMUNOSUPPRESION WITH 3D IN VITRO T-CELL ATTACHMENT AND EXOSOME CO-CULTURE IN DYNAMIC BIOREACTOR FLOW

A THESIS

SUBMITTED TO THE GRADUATE FACULTY

in partial fulfillment of the requirements for the

Degree of

MASTER OF SCIENCE

By

DANIEL SHAYANNE KARAMI
Norman, Oklahoma
2020

EXPLORING IMMUNOSUPPRESSION WITH 3D IN VITRO T-CELL ATTACHMENT AND EXOSOME CO-CULTURE IN DYNAMIC BIOREACTOR FLOW

A THESIS APPROVED FOR THE
STEPHENSON SCHOOL OF BIOMEDICAL ENGINEERING

BY THE COMMITTEE CONSISTING OF

Dr. Vassilios I. Sikavitsas, Chair

Dr. Matthias U. Nollert

Dr. Roger G. Harrison

ACKNOWLEDGMENTS

To begin, I would like to thank my advisor and principal investigator Dr. Vassilios Sikavitsas. Not only has he put his faith in me to bring a new project and direction to the lab, but he has spent countless hours working with me to educate ourselves on the new subject and work as a team to bring this direction to our lab. He has always been a guiding force, not only in lab, but also life, with great insights on how to think about problems, and phenomenal stories as well. I would also like to thank my committee members, Dr. Ulli Nollert and Dr. Roger Harrison. Dr. Nollet has been a life mentor for many years and someone who I keep coming to for advice on life and problems that I encounter or am curious about—although I don't ever read his book recommendations. Dr. Harrison has been a great leader and resource in my time in the lab, and also gives the best fist bumps.

The CBME AND SBME departments have been great help in both being supportive forces, but also for their help navigating through the collegiate process. CBME has always been a home since my undergraduate days, and with my lab located in their area of campus, I have had the pleasure of getting to know the staff and professors who felt like they wanted me to succeed. SBME, although a new department, has had phenomenal professors and staff that I have had the pleasure the work with and get to know like Dr. Rachel Childers, Dr. Stefan Wilhelm, Dr. Handan Acar, Shayla Glover, and Cherie Hudson. Alongside the department staff are the graduate students among them that have supported me. Michael Felder, Montana McGinnis, Charles Bagarie, Alexis Woodward, Nathan Donahue, Brandon Abbot, James Buerck and many others have helped me so much along the way and I appreciate all of their friendships so much.

And finally, I would like to thank my family for their love and support. My dad, mom, and sister have been there at every point in my life to keep me going and telling me how proud they are of

me. I would not be the person I am today without my family to guide me and give me their unfiltered opinions. I love all of you so much and will keep moving forward to make you all proud.

TABLE OF CONTENTS

LIST OF FIGURES

ABSTRACT

Cancer is a prevalent disease that impacts many lives all over the world, projected to pass more than 27 million deaths in 2030. Among many cancer therapies and treatment solutions are immunotherapies that include immune checkpoint inhibitors, T-cell therapies, monoclonal antibodies, and immune system modulators; however, the induced immune response has often been found to decrease significantly with time. Exosomes, typically 30-100 nm diameter vesicular bodies produced in the endosomal compartment, are produced by every cell in the body and found in almost every bodily fluid, which is also true for cancerous cells and tumors. Exosomes not only mimic the parental cell's membrane as they are released, but also are loaded with bioactive molecules like RNA that interact with neighboring cell population and even downstream cells and environments. Cancer cell-released exosomes have the capacity to interact with the immune system including CD8+ T-cells that are often responsible for many of the cytotoxic responses in the body. Such interactions have been hypothesized to be involved in the suppression of T-cell activity providing the potential explanation for the immunosuppressive properties of some cancers. As the exosome field of study is in its infancy, the interaction of exosomes with T-cells have been studied mostly in 2D cultures, but such studies have not managed to fully recapitulate the complex microenvironment and observations obtained from in vivo models. The development of more complex 3D culture environments and components that mimic the natural microenvironments where exosomes interact with T-cells is expected to provide cell responses closer to those observed in vivo.

Tools developed within the area of regenerative medicine and tissue engineering, including advanced 3D cell culture systems, have gained interest by cancer researchers as they assist in adding components that better mimic the physiological environments where exosome-T-cell

interactions take place. 3D flow perfusion is one such platform that incorporates the component of fluid flow present when T-cells interact with exosomes. Biomimetics also allow the modification of porous scaffolds, improving the ability of cells to recognize specific motifs such as the RGD binding motif that can be recognized by T-cells. Immobilizing T-cells via the RGD motif allows the creation of an immobile cell structure that can be exposed to exosomes through flow.

Poly-L-Lactic Acid (PLLA) 2D disks and 3D printed porous scaffolds have been generated and surface modified with Poly-ε-Cbz-L-lysine (Poly K) using an acetone-based partial solubilization approach that have been further modified using amine coupling allowing the incorporation of RGD adhesion peptide on the surface in a controllable manner. Increasing numbers of CD8+ T-cells attached onto the surface of both 2D modified disks and 3D printed modified scaffolds as the surface density of RGD increased. Activated human CD8+ T-cells secrete interleukin-2 (IL-2), a white blood cell regulatory cytokine, for which release has been shown to decrease significantly, or even get silenced, by the presence of exosomes from cancer cells. The decrease in IL-2 production is linked with the deactivation of T-cells and can be related to the immunosuppressive properties of exosomes.

When co-cultured with exosomes from H1299 (human non-small lung carcinoma) and A549 (human adenocarcinomic alveolar basal epithelial) cancer cell lines, T-cells showed decreasing IL-2 production when increasing the exosome to T-cell culture ratios from a 1:1 to 1:1000 ratio. A 1:10 ratio of T-cells to exosomes was sufficient to completely silence the IL-2 production of T-cells under 2D static conditions, while in a flow perfusion bioreactor with the presence of a

0.15 mL/min flow rate, or a superficial velocity of 1.2±0.5 mm/min, a higher ratio of exosomes of 1:1000 was necessary to elicit the same response indicating significant differences between the two culturing systems. Higher flow rates have resulted in almost 70% T-cell detachment, and for that reason exosome T-cell interactions were not explored within that flow regime. RGD modified surfaces resulted in T-cell immobilization with cells having a diameter of 7 – 7.5 μm for RGD densities of 0.27±0.43 nmoles/mm^2 and below. Higher RGD densities resulted in T-cells occupying a significantly smaller surface area resulting in diameters as low as 5 μm and for that reason were excluded from the study of exosome T-cell interactions under 3D flow perfusion. Our system provides a tool that can be used in exploring the interaction of exosomes with T-cells, the potential generation of exosomes in real-time by cultured cancer cells that can interact with downstream T-cells, or even test chemotherapeutic agents that may prevent T-cell silencing and provide a useful screening tool for the cancer research community.

1. INTRODUCTION

1.1 Relevance of Cancer and Cancer Research

In 2015, worldwide cancer cases had already reached more than 17 million alongside more than 8 million deaths. Between the 10-year gap from 2005 to 2015 the rate of cancer related deaths and cases increased by more than 30% which were partly due to population aging and increased birth rates. Cancer is currently the second leading cause of worldwide deaths and by 2030 is expected to exceed more than 27 million deaths [1]. Cancer impacts not only the lives of patients, their families, and their friends, but also adds an additional burden and socioeconomic problem to already existing ones in society with daily habits and aging like sedentary lifestyle, smoking, substance abuse, and alcoholism [1, 2]. The most common and notable cancer treatments are radiotherapy, surgery, chemotherapy, targeted therapies, and immunotherapies [3]. The current landscape of cancer research spans many countries and shows that cancer is an interinstitutional topic with advanced countries having higher research densities [4].

1.2 Introduction to Exosomes, Cancer, and T-Cells

1.2.1 Introduction to Exosomes

Exosomes are small vesicles that have been strongly implicated in cancer related processes. Exosomes typically range from 30 – 100 nm in diameter and are exuded by every cell line in the body, both normal and cancerous, involved in either communication and housekeeping, and were discovered almost 30 years ago in 1983 [5]. They are characterized as multivesicular bodies and they are the only types of extracellular vesicle that are loaded with intercellular contents fused with the parent cell plasma membrane before being sent into the extracellular matrix (*ECM*) and extracellular space [6-8]. Exosomes originating from healthy cells can be found in a wide range of bodily fluids like amniotic fluid, plasma, urine, blood, saliva, and synovial fluid [9-11]. The parent cell dictates the exosomal content, and as a result, cells of different phenotypes produce

exosomes with varying synthesis and compositions, and include biomolecules like tumor suppressing and transcriptional proteins, ribonucleic acids (*RNA*) like micro-RNA and non-coding RNA, deoxyribonucleic acids (*DNA*), [12, 13], and lipids [14-17]. Exosomes that have been circulating around their microenvironments contain such biomolecules that have the capacity to influence and transfer oncogenic properties and traits from cancerous to healthy cells, reaching even cells that can receive their contents in distant organs [18]. Cancer metastasis, or the spreading of cancer from its original location to other parts of the body, has been linked to the activity of exosomes by a theory proposed by Abdouh et al called genometastasis [19]. Recent studies have reaffirmed the contribution of circulating exosomes to cancer metastasis and their effect on oncogenic cell mutations [20, 21].

Although it has been 30 years since the discovery of exosomes, the exosome field is still in its infancy and the question of the exact role of exosomes in tumor progression and metastasis is still unclear due to their submicron size and complexity of their interactions [22]. Exosomes from cancer cells have been shown to create cancerous cells from other healthy local epithelial cells and invade the nearby extracellular matrix [23]. As mentioned earlier, exosomes exuded from cancer cells differ significantly from normal cells. Both their contents and rates of dispersal have been shown to differ. In 2014, a study compared breast cancer cells to normal mammary epithelial and showed that the breast cancer cell line exuded exosomes at almost two orders of magnitude greater compared to the normal cells. Several other studies have revealed similar findings showing increased exosome concentration in vitro and in vivo in animals and humans [24, 25]. Exosomes released from cancer cells, unlike normal cells, exude RNA-induced silencing complex, or RISC, complex-associated mRNA and this complex is essential to targeting and silencing genes [23]. The mechanism for exosome biomolecule content loading and

sorting, until recently, was considered independent from the cellular microenvironment. Indications have appeared that the exosomal secretion rates and exosomal uptake rates were increased in cancer patients when compared to healthy patients [26-28], implying that the tumor microenvironment influences them significantly [25].

1.2.2 Drug Resistance

Drug resistance, both innate and acquired, remain a cancer hallmark and a major challenge and obstacle for research to provide therapies and successful patient outcomes. Multiple studies have shown that cancer cell exosomes impact and modulate chemosensitivity by transferring chemoresistance to nearby recipient cells by transport of bioactive molecule like RNAs [29]. It is suggested that the microenvironment acidity stimulates exosomal output and these increased output rates elevate the rate of phenotypic transfer and impact drug influence and control antiapoptotic cycles [30, 31]. Innate multi-drug resistances, or *MDR*, are commonplace in cancer since cancer cells over express drug efflux pumps, transporters, and resistance proteins while acquired drug resistance is tied to a signaling pathway through the tumor microenvironment heavily populated by exosomes [32]. Given the central role of exosomes in cell-cell communication, they are linked to the resistance of cancer therapies to drugs, but not only in intuitive ways like gene transfer or microenvironment signaling [33], but also via cytotoxic drug sequestration in vesicles and their further expulsion to negate their effects [34, 35].

1.2.3 Immunosuppression

As exosomes impact their microenvironment with their transfer of bioactive molecules and drug resistances, they inevitable interact with the immune system. Both the innate immune system and adaptive immune system function alongside the tumor microenvironment and have a role that naturally hinders tumorigenesis. While chronic inflammation provides a perfect environment for

cancer promotion, like hypoxia and low pH, the immune system seeks and destroys neoplastic cells and this interplay has been defined as cancer immunosurveillance [36-38]. This recently explored hypothesis [38] implicates three main factors of the immune system with tumors: (1) elimination of neoplastic cells, (2) the establishment of equilibrium between the growth of tumors set by the balance of cancer cell elimination by the immune system and tumor growth, and (3) the upregulation of more immune-privileged cancer cells through natural selection. The fundamental step of the immune response is antigen presentation which comes when macrophages and B-cells that are bound to major histocompatibility complexes (*MHC*) Class I and II (CD8+ for cytotoxic T-lymphocytes (*T-Cells*) and natural killer cells and CD4+ for helper T-Cells, respectively) present antigens for their respective lymphocytes and bind which forms a immunological synapse[39]. Cancer cells primarily interact with by the cytotoxic and natural killer cell with CD8+ T-lymphocytes [39]. The regulatory role of exosomes has recently appeared in the literature involving their regulation of the synapse formation between antigen-presenting cells and T-cells, promoting an immune response that may play a role in inhibiting immunosurveillance [40-42].

Exosomes interact with the immune system in four distinct ways: (1) direct antigen presentation of cells presenting the antigen synapse [43], (2) indirect exposure by ‘decorating’ with a phenomena cross-dressing which repurposes nearby completed synapses to escape the immune response [44-46], (3) internalized by the antigen-presenting cell (*APC*) and then influence the presented markers on the same APC [46], and (4) after internalization impact the exosomes secreted by the APC that further interact with the immune system [47]. As every nucleated cell expresses molecules for MHC Class I, their respective exosomes do as well because of the surface antigens obtained from the parent cell membrane such that they are able to interact with

the cytotoxic lymphocytes and natural killer cells [48]. Cancer-related antigens are contained in tumor-derived exosomes that may initiate an immune response and multiple studies [49-51] suggesting that tumor-secreted exosomes can also become antigens for interaction with CD8+ T-Cells indirectly through APC presentation and cross-dressing [50]. Exosomes may also release factors such as galectin 9 and Fas ligand which cause apoptosis to nearby immune cells [52-54]. These factors are once again tied to the bioactive carriers within exosomes which have also been shown to impact natural killer cell immunity [55] and work by transferring micro-RNA to recipient cells [56, 57]. Such deactivation can be linked to the inactivation of the T-Cells and the respective downregulation of some cytokine productions like interleukin-2 (*IL-2*) or TNF-α or upregulation of IL-6 [58].

1.3 Challenges of Exosome and Cancer Testing

As the impact of exosomes on cancer has been clearly established in the oncological field, there is upmost importance to create a more realistic in vitro environment. Exosomes are exuded by almost every cell; however, mainstream exosome isolation only comes from a select few well-defined cell lines, so greater variety of sources are needed to generate a greater variety of information in biology [59]. Even though a universally accepted board for exosome research has been created called the International Society for Extracellular Vesicles (*ISEV*), important aspects are left to the investigators' opinions and discretions [60]. The culture conditions and extraction specifics play a large role in the impacts and effects on normal and cancer cells including the production rates from 2D vs 3D cell cultures [61], their passage number [62, 63], cellularity, and proximity to their cellular microenvironment [59, 62]. When transitioning from in vitro studies to in vivo studies, there is a large number of inconsistencies identified implying that in vitro studies require more attention [64]. Discrepancies have been shown when cancer cells are exposed to

drugs and results have been compared to in vivo experiments. Such discrepancies even exist between in vitro 2D settings and in vitro 3D settings. The study of exosomes in cancer biology inevitably will suffer from the same limitations.

1.4 Importance of In Vitro Testing

In vitro models create not only an ideal starting point for medical and biological research, but also an important subset, complimenting the more complex in vivo models. Results of in vitro testing should compare and verify more complex moieties, especially in vivo models and testing [65]. Both in vitro and in vivo models play important roles in cancer research by enabling drug screenings, testing therapies, and providing mechanistic insight for tumor growth and metastasis [66]. One of the many advantages of in vitro models is their ability to implement and understand multifactorial studies for more advanced systems [67]. While in vivo models more precisely showcase the complexity of the cancer environment, discerning, visualizing, and extracting data is not only challenging and difficult, but expensive as well [66].

The complexity of in vitro cancer models of tumors varies and range from 2D monocultures to the 3D multicellular structures and microenvironments [68]. The development of 2D models has historically provided insight on growth, proliferation, migration, and drug effectiveness, to name a few [69, 70]. Typical considerations are cell sources, extracellular matrix, and biochemical microenvironment [71] with some models even introducing perfusable systems [68]. But the ability for in vitro models to test multiple parameters is precisely their major advantage with a premise that these results are valid when tested in vivo. In vitro systems can be flexibly tailor-made to reduce in vivo variability. The easy implementation of a wide variety of cancer cell lines in in vitro culture system have made them attractive in biological studies [72, 73] as they manage

to match some of characteristics of tumors [74, 75], and as said earlier, certain discrepancies still remain necessitating in vitro models to reach a better agreement with in vivo studies.

1.5 2-Dimensional vs 3-Dimensional

The prevalence of 2D systems and cultures stems from their cost, reproducibility, and ease of use [76]. 2D monolayer testing has proven valuable for cell-based studies, but inconsistencies found between 2D in vitro systems and in vivo cultures create limitations for these in vitro settings [77]. The absence of ECM and the 3-dimensional tissue architecture found in in vivo tumors cannot be recapitulated by 2D cultures which often result in misleading findings that do not correspond to in vivo responses [78, 79]. Cancer cells reside in their natural microenvironment that include the local architecture and the specific ECM, experience specific 3-dimensional architectures that affect cell signaling, gene expression, and overall phenotype of cancer cells [80-82] with the presence of vascularization and tumor specific ECM [83]. The 3D microenvironment affects stem cell differentiation [84, 85] and it has been also shown to influence the phenotype of over 100 cancer cell lines [86]. Changes in cancer cell gene expression and responses to circulating biomolecules have been attributed to the specific microenvironment these cells reside in [87].

3D systems and cell cultures have been shown to mimic the natural tumor microenvironment more closely and are expected to recapitulate the in vivo cancer cell phenotype more reliably [77]. The physical and spatial characteristics of the cancer cell microenvironment impact its signal transduction and alters multiple signaling cascades, which allows 3D cultures to generate responses closer to those in vivo [88, 89]. Proliferation rates between 2D and 3D cultures vary and are dependent on the type of surface they are attached to, the culture media, cell density, the presence of secondary cell types, among others, and reduced proliferation rates have been

reported in some 3D cultures compared to 2D [90-92] while in others the reverse behavior has been observed [93]. The cultivation of cancer cells in 3D systems for cancer cell biology and stem cell and drug discovery studies hold great promise and move in vitro studies towards the final goal to mimic the behavior observed in natural in vivo tumor microenvironments [94, 95].

1.6 Importance of Synthetic Scaffolds and Surface Modification

1.6.1 Types of Scaffolds

An ideal 3D system would mimic the pathophysiological and physiological microenvironments so that cell cultures could differentiate and proliferate, producing a model that could induce cell-cell interactions and cell-ECM interactions, waste management and tissue-specific ECM [96]. The most promising models for in vitro cancer analysis are spheroids, organoids, and scaffold-supported bioreactor models [97], borrowing many of these models from tissue engineering. Spheroid models are commonly used for 3D tumor models and have made advancements in the field such as chemoresistance [90] and gene expression [98], but these models neglect important stressors for tumor progression by culturing them in static systems [99]. Fluid flow and interstitial shear forces have been shown to play a critical role in mimicking in vivo biomechanical forces in vitro not only in several normal cell types [100], but in tumor cells as well [101, 102].

Another recent addition to oncological culturing is the use of organoids, which are self-organizing tissue-derived stem cells that form organotypic structures [103] and can even be derived via induced pluripotent stem cells [104]. Although organoids present worthwhile benefits, their limitations to full-scale modeling reduce their viability. Organoids lack the development of vessels, immune cells, and stroma [105], and their interaction with serum and serum-derivatives cause unfavorable long-term results [106]. Unreliable growth and

heterogeneity between organoid samples [107] yield undesirable conditions for macroscale modeling.

1.6.2 Scaffold-Supported and Polymers

Tissue engineering typically involves cell-scaffold constructs with scaffolds having specified bulk and surface properties as required by the maturation rate of the tissue construct [108, 109]. Scaffolds with ideal characteristics and properties help develop an environment where certain surface properties increase compound and molecule affinity [110]. Scaffold-based models have shown to more accurately mimic cell-ECM characteristics and interactions compared to other 3D techniques [111].

The challenge of mimicking tumor microenvironments stems from their environmental complexity. 2D morphologies differ from their 3D counterparts in matrix stiffness and ECM properties which alter molecule diffusion [96] and reinforce that cellular heterogeneity is present in environments with varying differentiation and proliferation rates [112, 113]. The disparity between native morphologies and 2D systems can be solved by using 3D constructs from synthetic and natural materials [96]. 3D models expand on 2D system and can better replicate tumor properties [114, 115] where natural scaffolds, like collagen and hydrogel, are commonplace in tumor engineering due to their relevance on physiological properties [116, 117]. However, natural scaffolds present limitations that range from low modularity and batch material inconsistencies to bioactive site variability and poor cell interactions in dynamic flow-based environments [118]. Synthetic polymers, like poly lactic acid (*PLA*), poly glycolic acid (*PGA*), and poly caprolactone (*PCL*) are alternatives to natural scaffolds and present solutions for their limitations [119]. Scaffold architecture and geometric control can be achieved with 3D printing and can provide desirable ECM properties [120] and alleviate batch variability [121]. Even

though polymers exhibit biodegradability and biocompatibility [118], some disadvantageous properties, like hydrophobicity and reduced cell-adhesion, require further consideration.

1.6.3 Surface Modification

Biological, physical, and chemical properties among synthetic scaffolds can be optimized to improve the interactions between the scaffold material and cells [122]. Surface modification is creating small modifications on the surface of a material to present desired physical or chemical characteristics without affecting the bulk compound properties. Synthetic polymers can utilize proteins and peptides which enhance cellular proliferation due to elevated cell adhesion and ECM development [123-125]. The modification of the polymer surface has the ability to improve the degradation rate, biocompatibility, bioactive molecule permeability, and mechanical property of the material [126].

Cell-matrix and cell-cell interactions impact the rate of tumor proliferation and progression based on cell morphologies which are dependent on cell-adhesion [127, 128]. Cancer cells exhibit weaker cell adhesion properties and fewer bioactive sites [129, 130] which can be alleviated with common surface moieties for adhesion like cadherins [131] and peptides [120]. Synthetic scaffolds have appeared as a means to navigate 3D models for cancer by creating more uniform and controlled adhesion platforms [118]. Oral squamous cell carcinoma [132], breast cancer [133], and ovarian cancer cells lines [134] have been reported to show increases in in vivo characteristics like cellular penetration, angiogenic abilities, metastases, cell adhesion, and cell seeding when cultured with modified synthetic scaffolds.

1.7 Importance of Flow Perfusion and 3D Macroscale

Fluid flow and shear rates provide beneficial dynamic environments for cellular culture and modeling and are showcased in the oncological field with microscale systems. Microfluidics have been commonplace in the oncological community for its modeling based on microscale control of laminar flow for nutrient and compound transport [135, 136] and cell characteristics and pharmaceutical properties and interactions [137]. Cell sorting [138] and pharmacodynamic studies [137] have been using microfluidics as an effective analytical tool for tumor biology. Microfabrication techniques like microcontact-printed scaffolds have noted better control over surface chemistry and topography [139]. Large 3D systems are often used to produce and obtain microscale models by providing uniform growth, distribution, and viability while reducing experimental variabilities [140-142]. 3D constructs, like immobilized hydrogels, have been used to investigate microfluidic and microscale dynamics for tumor models [143, 144], but diffusion cannot be controlled as closely with natural scaffolds when compared to porous scaffolds, like synthetic polymers [145].

Macroscale flow-perfusion bioreactors may be an appropriate next step to more accurately model tumor progression since tumorigenesis is a delicate balance of both macroenvironmental and microenvironmental aspects [146] wherein the functional connections between cancer cells and their neighboring microenvironments can result in tumorigenesis [147] and phenotypic alterations [148]. Differences in cellular responses are observed when comparing microfluidic systems to biological assays and their macroscopic counterparts [149, 150]. Increased cell viability and nutrient availability was observed for macroscopic systems, and the volume densities varied as much as 5 times between scales [150]. Biomimetic tumor models using porous scaffolds [151, 152] and tumors of musculoskeletal origin [153, 154] have been

successfully modeled with macroscale perfusion systems and these same systems have been shown to obtain comparable in vitro pharmaceutical responses in tumors [155, 156]. When compared to static 3D cultures, flow perfusion has been shown to increase cell proliferation and cell homogeneity within tissue-like structures and exhibit morphology and phenotypes like xenografts [155]. Biomechanical stimulation due to shear stresses has been often overlooked as a means of tumor progression [157, 158] and 3D macroscale systems present a controlled in vitro environment to explore these dynamic conditions.

1.8 Project Goals and Set-Up

1.8.1 Scope

The scope of this project involves in vitro modeling, cancer research, and immunology. There are substantial differences between 2D and 3D models based on nutrient availabilities, gene expressions, cell viabilities and densities, morphological and phenotypic changes, and most notably shear stress and fluid flow. The hurdles of 3D cancer modeling stem from the complexities of the microenvironment present around tumors. Spheroids, organoids, and natural scaffolds, like hydrogels, have limitations like geometric control, material inconsistencies, and unfavorable transport environments that struggle to accommodate dynamic flow conditions. Coupled with the high cellularity of tumors and localized stresses and gradients, 3D cancer modeling remains a challenge.

Polymeric scaffolds with surface modifications are equipped with advantageous properties to remedy the challenges present in 3D macroscale cancer models. Mimicking both the microenvironments and macroenvironments are vital to modeling cancer due to its importance in cell and ECM interactions. Polymeric scaffolds offer geometric control in 3D printing and bioactive features like biodegradability and bioavailability, and their adhesion limitations can be

alleviated using surface modifications. Common surface compounds like cadherin and peptides are important connective ligands in tumor environments and even further mimic the tumor environmental conditions.

Activated immune systems typically seen in cancer and infectious disease seem to be immunosuppressed in many types of cancer. Even therapeutic and genetic alterations, like CAR-T systems that reactivate the immune system, are subsequently silenced. The interconnectivity between MHC class I cells, like cancer, and the immune system showcases their environmental complexity. Exosomes exuded from cancer cells have been theorized to be linked to this immunosuppression as well as a host of other tumor traits like metastasis, increased proliferation rates, and genetic and phenotypic alterations. Inconsistencies are prevalent amongst the exosome field which imply that improved in vitro models are needed. In vitro models can provide reduced costs and introduce multifactorial environmental manipulation in shear rates and ECM developments and reduce variability with precise management of environmental conditions.

1.8.2 Goals

T-Cells play a pivotal role in both the immune system and in cancer; however, testing T-cell interactions in flow models can become difficult due to their suspension-based culture. Immobilization of CD8+ T-cells will better isolate interactions with circulating factors. The utilization of surface modification and attachment with peptides allow T-Cells to become immobilized onto a surface to mediate testing variability. A model that encapsulates the complex nature of the cancer and immunological macroenvironments and microenvironments would set a foundation for future testing and validation.

The goal of this project is to create a proof-of-concept 3D system to test exosomal effects on T-cells. The first steps are to create a surface modified 3D printed PLLA scaffold modified with RGD peptides to bind T-Cells. Subsequent steps are to devise indirect and non-invasive measurements to measure T-cell attachment and activation. These steps can be achieved together by measuring a cytokine produced from activated T-Cells called interleukin-2 (IL-2), which plays a pivotal role in T-Cell proliferation. Activated T-cells that are stimulated with specific compound called Tetra-deca-noyl-phorbol acetate, or *PMA*, produce IL-2 and deactivated or blocked T-Cells do not produce IL-2. High sensitivity ELISA kits can be used as an indirect quantification method for produced cytokines. The T-Cells would then need to withstand flow perfusion bioreactor conditions before exosome co-cultures in 2D and 3D. The expected response from the co-culture of cancerous exosomes is decreasing IL-2 production by T-cells due to their inactivation, blocking, or silencing.

1.10 Conclusion

The complexities of cancer mean that more in-depth models are needed to mimic their interactions. The goal of models is to create systems that mimics in vivo environments to test system conditions more cost effectively, more accurately, and with less variability. Exosomes and their impact on the body and nearby systems require more updated details. The use of 3D models can limit and eliminate inconsistencies found in in vivo trials while incorporating more complex dynamics like microenvironmental and macroenvironmental factors. The creation of a system to mimic the cancer biome would add not only cancer understanding, but also pharmaceuticals and drug therapies.

2. METHODS

2.1 2D Scaffold Preparation

2D poly-L-lactic acid, or PLLA, films were utilized due to their ease of access, high reproducibility, low cost of production, and their ability to generate 3-dimensional porous scaffolds in a reproducible way. The 2D films were prepared in accordance with procedures that have been previously published [159, 160]. PLLA (NatureWorks LLC; grade 6251D; 1.4% D-enantiomer, MW = 108,500 KD) pellets were used to produce the 2D films. Approximately 2.5 grams of PLLA pellets were weighed and then combined with a 35 mL of chloroform to dissolve. The pellets were mixed with a stir bar on a magnetic mixer for approximately 45 mins to completely dissolve to PLLA pellets. The heterogeneous mixture was then poured evenly into three 50 mm petri disks. The containers were set overnight at room temperature to evaporate.

After the evaporation step, 2D films of 50 mm diameter were collected. The 50 mm disks were then stamped using a fixed stencil into 8 mm disks. Each new scaffold was sterilized using 95% ethanol, allowed to sit in sterile PBS to leech off ethanol for 1 hour, and then stored into a vacuum chamber. Scaffolds were used for cell seeding within 24 hours from their sterilization.

2.2 3D Scaffold Preparation

2.2.1 Material

The method used to generate 3-dimensional porous PLLA scaffolds was 3D printing. In order to feed the polymer into the 3D printer, PLLA had to be in the form of a filament. Due to the absence of PLLA filaments free of additives the filament used was generated in-house.

As specialized extruder was used to produce this filament (the used extruder was owned by the Aerospace and Mechanical Engineering department at the University of Oklahoma). PLLA pellets were placed in the hopper of the extruder to heat up, and then extruded into a 1 mm

diameter filament. The filament was subsequently used in a 3D printer and, similar to the PLLA pellets, were vacuum stored after preparation. Prior to usage, 3D scaffolds were placed in a biosafety cabinet and purged of air with a syringe vacuum method in PBS, cleaned with 95% ethanol and then allowed to sit in sterile PBS to leech off ethanol for 1 hour.

2.2.2 Printing

The 3D printer used was the MakerBot® Replicator® Fifth Generation Desktop 3D Printer. The filament was placed and raveled in their provided filament cassettes and then attached to the rear of the machine. Print settings were used to provide the necessary conditions for not only the filament temperature, but also the extrusion diameter. The filament was placed into the extruder and heated to 195^{o}F, extruded to a 0.5mm diameter and placed at a rate of 0.5 cm/second. Scaffolds were printed in laddered extrusion patterns to produce a square 2 mm x 8 mm x 8 mm scaffold. 3D printed scaffolds were then stamped using the same stencil as with the 2D films. An image of both the printed and stamped 3D scaffolds seen in Figure 1.

Figure 1**: 3D Scaffold design from the starting square to the stamped 4 mm by 8 mm cylindrical scaffold.**

2.3 Surface Modification

2.3.1 2D PLLA Films

The protocol for the surface modification of the 2D films was similar to previously published procedures [159, 160]. 2D scaffolds were prepared as above. Each 8 mm disk was immersed with a 70:30 acetone aqueous solution of Poly-ε-Cbz-L-lysine (Sigma-Aldrich; Poly-ε-Cbz-L-lysine; MW = 500-4000 KD), which will now be referred to as *Poly K*, ranging from 1 mg/mL to 10^{-7} mg/mL. Films were placed in a shaker for 12 hours to promote the entrapment of the poly K mixture on the PLLA surface before being removed to be washed with 3 cycles of Triton X-100 and sterile PBS.

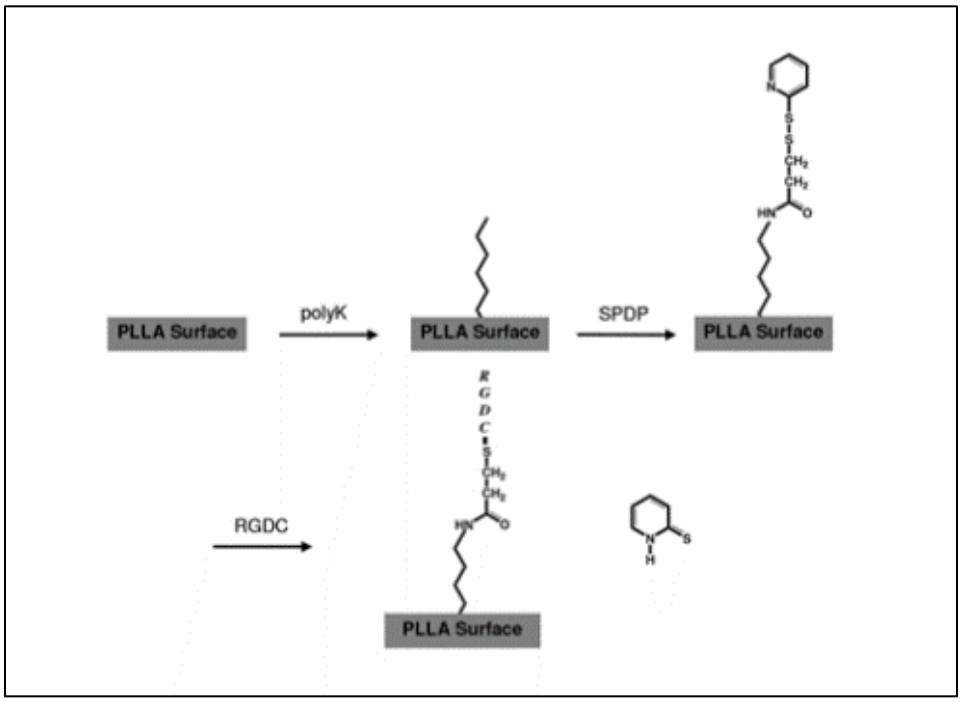

Figure 2: **Breakdown of surface modification starting with PLLA and adding Poly-lysine, SPDP And finally RGDC[159, 160]**

Poly K presence on the films was determined by a horseradish peroxidase (periodate-HRP) reaction with the amino acid chain. Films modified with poly K were reacted with 600 µL of 10^{-8} M of HRP (Thermo Fisher; 1-Step™ ABTS Substrate Solution) for 2 hours. The provided ABTS kit was used to determine the HRP presence at 405 nm on a Synergy HT Multi-Mode Microplate

Reader (Bio-Tek) with standard of measured poly K prepared for calibrations. Specified by the manufacturer, H_2O_2 and ABTS reagent were dilated with citrate buffer and then incubated with disks at 600 µL of the solution. Poly K decay on 2D films was tested by performing the HRP detection method on films that remained in the biohood at room temperature for a period of up to 7 days.

With poly K incorporated onto the surface of the films of the PLLA, a functionalization can occur to chemically bind, via amine coupling, the RGD peptide to the poly K that is entrapped onto the surface of the scaffold. Poly K modified disks were incubated with 600 µL of 1 mM *SPDP* (Thermo Fisher; SPDP (succinimidyl 3-(2-pyridyldithio)propionate); MW = 527.57 KD) in HEPES buffer for approximately 30 mins. Similar washing cycles with Triton X100 and sterile PBS were used after the linking. The disulfide bond present in SPDP was utilized with a disulfide reduction to place the RGDC onto the surface. SPDP-linked scaffolds were then incubated with 600 µL of 100 µM RGDC (AnaSpec; Cell Adhesive Peptide [RGDC]; MW = 449.5 KD) for 1 hour and rinsed as in the previous steps. A breakdown of the chemistry of the surface can be seen in Figure 2. The subsequent reaction released pyridine-2-thiol can be seen at a wavelength of 343 nm and can be used to determine the concentration of reacted RGD.

2.3.2 3D Scaffolds

Porosity of the 3D printed scaffolds was found to be 85% and was obtained with the scaffold weight, material density, and structure volume. 3D scaffolds were modified following the same protocol as the 8 mm 2D films by modifying the procedure of the entrapment of poly K and incorporation of RGD. The presence of the 3D porous network that needed to be accessed by the poly K and RGDC moieties during their respective scaffold incorporation necessitated the use of

vacuum. 3D printed scaffolds were placed in a glass vial with each concentration of poly K and then vacuumed repeatedly with a needle syringe. Subsequent steps using SPDP and RGDC were done using the same vacuum method and each step was allowed to proceed for the same time period as the one used in 2D films. After modification, scaffolds were left in sterile PBS in a biosafety cabinet and used within 24 hours.

2.4 T-Cell Culture and Preparation

Human CD8+ T-Cells were obtained from StemCell Technologies (StemCell Technologies; Human Peripheral Blood CD8+ T Cells, Frozen; $1x10^7$ Cells per vial). As cells were labeled, profiled, and documented from the same donor designated by StemCell Technologies, T-Cells were used directly from storage. T-Cells were placed into RPMI 1640 (Thermo Fisher; RPMI 1640 Medium) with 1% anti-anti and 10% fetal bovine serum to clean their contents and then centrifuged at 1000 RPM for 3 mins before resuspended in the anti-anti FBS RPMI 1640 media. To determine the exact number of T-cells used in calibrations, flow cytometry was used on the T-cell samples before use.

2.5.2 Platform Set-Up

2.5.1 Static 2D and 3D Set-Up

Static conditions for attachment, spreading, and exosomes co-cultures were tested using 48-well plates. 2D PLLA films were placed into their respective wells. Working volumes for T-cell attachment and exosome co-culture for static conditions were 1 mL. 3D static scaffolds also used the same set-up of a 48-well plate. 3D static scaffolds were placed into their respective wells and 1 mL working volumes were used.

2.5.2 Bioreactor Set-Up

The bioreactor main body and cassettes were set up prior to use. The bioreactor system was sterilized 3 days prior and allowed to vent fumes before proceeding. The system was operated and purged of air in a biosafety cabinet and set in a 37^{o}C incubator to reach equilibrium temperature for 6 hours. When equilibrated, prepared 3D scaffolds with attached T-cells were placed into each cassette while in the biosafety cabinet. Separate flow rates were used based on the peristaltic pump specifications. The lowest and highest achievements flow rates used were 0.15 mL/min and 1.5 mL/min. Each cassette was connected to its own vial of media and had a working volume of 5 mL of anti-anti FBS RPMI 1640 media. For flow rate testing the bioreactor system was connected to a single reservoir to accommodate necessary working volumes for the system and can be seen in Figure 3.

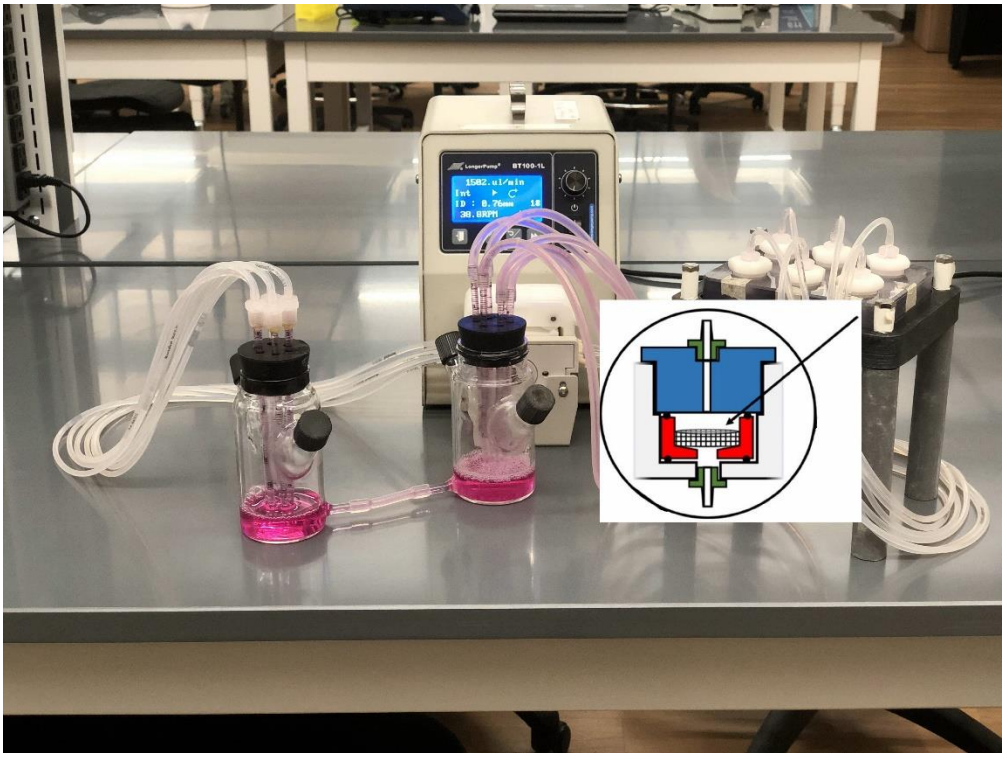

Figure 3: **Mock bioreactor set-up for flow perfusion testing. A reservoir container is linked to the pump with tubing, and then to the insert of the scaffold cassettes and finally toward the outlet to another container. The inset shows the inside of each of the 6 chambers. The scaffold is form-pressed so assure that fluid flows through the porous structure and not around, with the inlet above and outlet below.**

2.6 PMA Preparation and Stimulation

2.6.1 2D PLLA Films

2D 8 mm films were carefully cleaned of previous anti-anti FBS RPMI 1640 media and prepared for cytokine stimulation. PMA (Sigma-Aldrich; 12-O-Tetradecanoylphorbol 13-acetate; MW = 616.83 KD) was used to stimulate activated T-Cells to produce IL-2. A 10 µM concentration of PMA in the anti-anti FBS RPMI 1640 media was created and then reacted with the 2D films for 4 hours. To minimize potential contaminates like T-cells or scaffolding, the samples were taken and centrifuged at 1000 RPM for 3 mins and the supernatant used for cytokine analysis.

2.6.2 3D Printed Scaffolds

Static 3D scaffolds were stimulated similarly to the 2D 8 mm films. A 10 µM concentration of PMA was used on the 3D scaffolds and stimulated for 4 hours. Samples were centrifuged and the supernatant used. 3D scaffolds used in the bioreactor system were ran and stimulated with PMA. The collection process was similar to the static 3D scaffolds.

2.7 Exosome Preparation and Co-Culture

2.7.1 2D PLLA Films

Human-derived cancer exosomes were obtained via a collaborating lab—Dr. Ragajopal Ramesh at the University of Oklahoma Health Science Center. Exosomes from two different cancer cell lines were used: (1) exosomes from *H1299,* a human non-small cell lung carcinoma cell line and (2) *A549*, an adenocarcinomic human alveolar basal epithelial cell line. The concentrations of each exosome were 1.75×10^{10} exosomes/mL and 2.83×10^{9} exosomes/mL. Exosomes were diluted from their initial concentrations to 10^{3} exosomes/mL to be used in exosome ratios with T-cells. Ratios of 1:1, 1:5, 1:10. 1:20, and 1:100 T-cells to exosomes were used to test exosomal properties on T-cells. 2D films were incubated concurrently with exosomes.

2.7.2 3D Printed Scaffolds

Static 3D scaffolds were cultured similarly to 2D 8 mm films. However, for the flow perfusion bioreactor system, the concentration of exosomes was extended and tightened to reduce testing capacities based on bioreactor sample availabilities. Exosomes concentrations ranged from 1:10 to 1:100 and 1:1000 T-cells to exosomes. Exosomes were incorporated into the anti-anti FBS RPMI 1640 media and circulated while testing under the lowest flow condition of 0.15 mL/min.

2.8 IL-2 Indirect ELISA

An IL-2 ELISA kit (Abcam; Human IL-2 ELISA Kit High Sensitivity) was used to detect IL-2 production from PMA-stimulated T-cells. The assay was performed via the manufacturer's instructions. Samples and standards were prepared, and the assay wells prepped. The antibody linkers were placed into each well and the functionalization was underway. Washing buffer was used in triplets after each subsequent step. After functionalizing, the dye buffer was used, and the results were recorded at 450 nm.

2.9 Statistics

Following data collection and analysis, a one-way ANOVA was conducted to determine if there was a significant effect (p-value < 0.05). The number of samples ranged from 3 – 9.

3. RESULTS AND DISCUSSION

3.1 Introduction

Results will be presented sequentially to accommodate research flow. They will appear similar to the material and methods. 2D testing will be followed by 3D testing. Surface modification will lead into T-cell attachment followed by bioreactor use and finally exosome co-culture. For ease of access, all surface modified films and scaffolds will be designated by their initial solution concentration of poly K used for entrapment followed by the RGD modifications.

3.2 Surface Modification with 2D Films

3.2.1 2D Poly K Entrapment

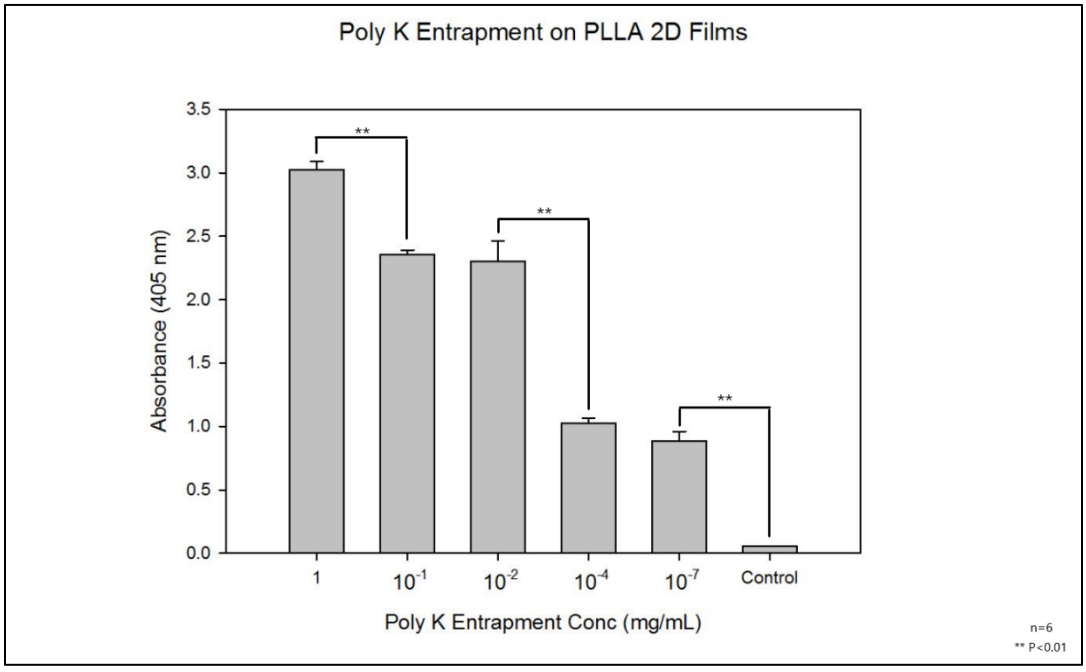

Figure 4: **Poly-K entrapment onto 8 mm 2D PLLA films (n=6). Concentrations range from 1 mg/mL to 10^{-7} mg/mL in 70:30 acetone and water.**

Poly K entrapment levels are presented as shown in Figure 4 as they relate to the entrapment process via the Poly K solution. There is a significant difference between the highest Poly K entrapment concentration of 1 mg/mL and the next highest at 10^{-1} mg/mL. The higher solutions at 10^{-1} and 10^{-2} mg/mL do not show significant differences of Poly K entrapment; however, as

lower concentrations Poly K are used, significant differences appear. Historically, these trends have seemed to demonstrate that above a starting solution of Poly K 10^{-2} mg/mL exists a saturation point; however, these trends could have been due to steric hindrance of the detection of the HRP with the maleimide used to identify the entrapped Poly K on the surface of the material; however, such saturation has been suggested that was due to the steric hindrance was not validated by our results. The immediate trend that comes from the Poly K entrapment is that as you increase the entrapment concentration that there is an increased entrapment of Poly K on the surface of the synthetic polymer. To better compare to historical data, these films were modified and tested on freshly made scaffolds.

3.2.2 2D Poly K Entrapment Stability

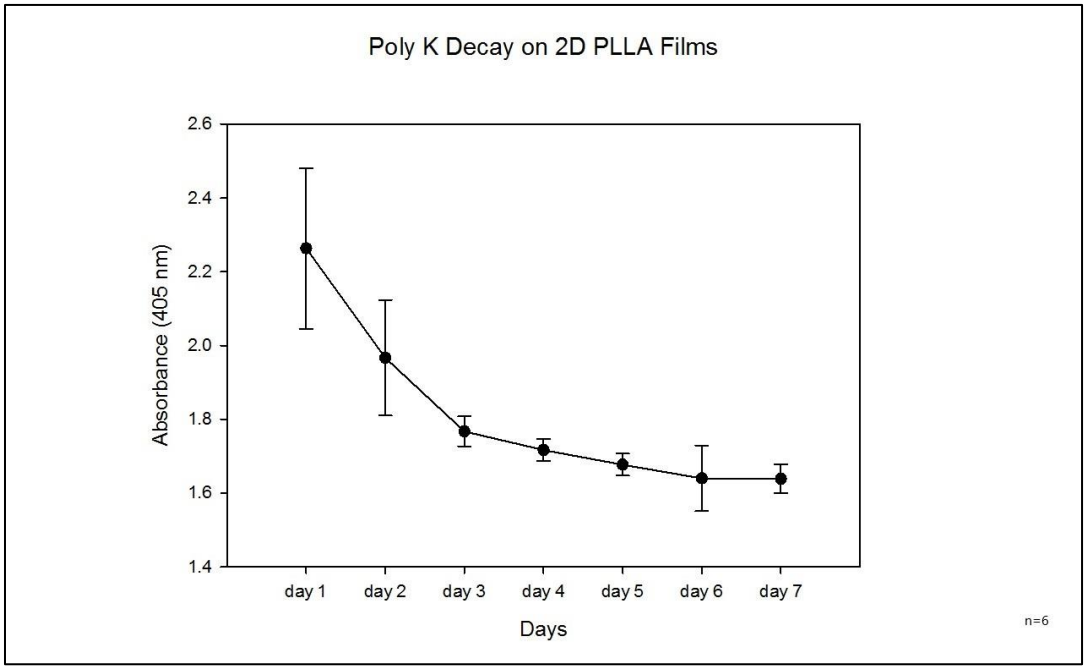

Figure 5**: Poly K decay over a 7-day period to test detachment of absorbed Poly K on PLLA films (n=6). Based on this graph, every scaffold and film had been stored for 4-days prior to use for the poly-k on each would stabilize.**

Poly K stability requires consideration because poly K is not chemically attached to the PLLA but simply entrapped by the partial solubility when exposed to the acetone solution. Surface

erosion has been observed for a 7-day period. A steady decrease from day-1 to day-4 was observed where day-4 and day-7 present no significance differences denoting that a stable entrapment can be accomplished if the surfaces generated are left for a 4-day period. As such, all subsequent surface modification steps were performed after a 4-day resting period in sterile PBS to ensure a stable Poly K and peptide surface not suffering from further decay. The observed decay during the first 4-days after the prepared PLLA surface is attributed to potential physisorption beyond the expected entrapment.

3.2.3 2D RGD Amine-Coupling

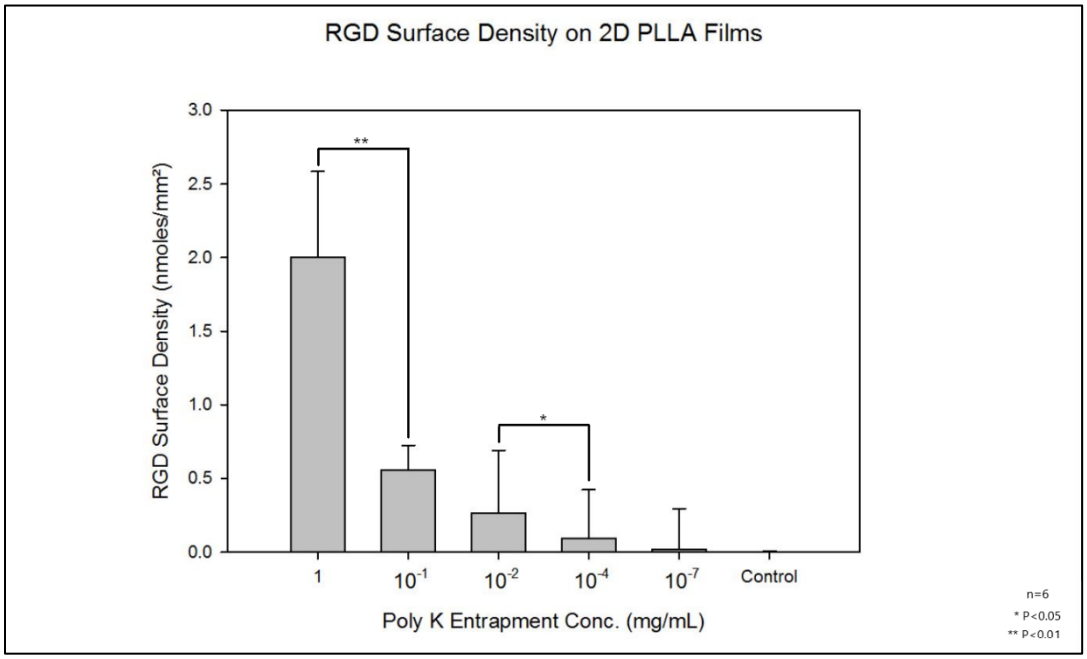

Figure 6: **RGD amine-coupling onto 2D 8 mm PLLA films (n=6). 600 µL of 100 µM RGD was added to concentration of poly K seeding that ranged from 1 mg/mL to 10^{-7} mg/mL.**

RGD has been attached on the Poly K surface via amine coupling which has allowed further modification to present the RGD peptide on the surface. Different Poly K entrapped surfaces have been used, characterized by the level of Poly K in the solution when partial solubilizing with the acetone solution. Those levels varied from 1 mg/mL to 10^{-7} with a control group that contained no Poly K. As seen above in Figure 6, there is a significant difference between 1

mg/mL and 10^{-1} mg/mL, but there are no significant differences ($P < 0.01$) on the RGD entrapment between 10^{-2} and downward toward the control. There was a difference ($P<0.05$) with 10^{-2} and 10^{-4} mg/mL, which does seem to corroborate the trends seen in the Poly K entrapment. The RGD surface density range from 2.00±0.58 nmoles/mm^2 for 1 mg/mL to 0.02±0.28 nmoles/mm^2 for 10^{-7} mg/mL. The possible saturation points in the 2D Poly K entrapment concentrations do not seem to be present with the response of the 1 mg/mL modified film with a larger increase between 1 mg/mL and 10^{-1} mg/mL. On the lower end, the lowest level of Poly K entrapped surface did not show an expected difference with the control surface, contradicting the results in Figure 4 which would mean that the further modification of the Poly K generated significant difference had been observed from the 10^{-7} mg/mL surface to the control. It needs to be reiterated that the entrapment in Figure 4 were with freshly modified surfaces while the results in Figure 6 were rested to account for physisorption. As said in Figure 4, it is possible that the majority of Poly K detected on Figure 4 for the 10^{-7} mg/mL solution-Poly K generated surface had been physiosorbed and has been detached from the period and now allowing the lack of a significant difference for the RGD between the lowest Poly K entrapment concentration and the control. A similar trend appears in that an increase in the Poly K entrapment concentration increases the RGD surface density.

The Poly K used in solution to entrap does seem to entrap more Poly K onto the surface on the surface of the films, such that there is an increased binding and reaction with the RGD after functionalization. An attempt was made to evaluate the RGD levels attached on the PLLA surface using the disulfide reaction with SPDP, as traditionally the RGD quantification was done via the absorbance of the pyridine-2-thiol. The absorbance of the release of Pyidine-2-Thiol can be tested the indirectly measure the RGD reacted on the surface of the Poly K modified films.

Although the absorbances for the released pyridine-2-thiol do not show large deviations, the dose response curve generated incorporated quite a bit of data noise. The RGD surface densities were found using the same dose response curve found in the appendix with Figure 20. The nmoles of RGD range from 100±29 nmoles to 1±13 nmoles from 1 to 10^{-7} mg/mL as can be seen in Figure 6 and were corrected with the surface area of 50 mm^2 for the films to 2.00±0.56 to 0.02±0.28 nmoles/mm^2. To simplify the classification of each surface modification, the average RGD surface density will be used to signify the Poly K entrapment and the subsequent RGD functionalization.

3.3 Surface Modification 3D

3.3.1 3D RGD Amine-Coupling

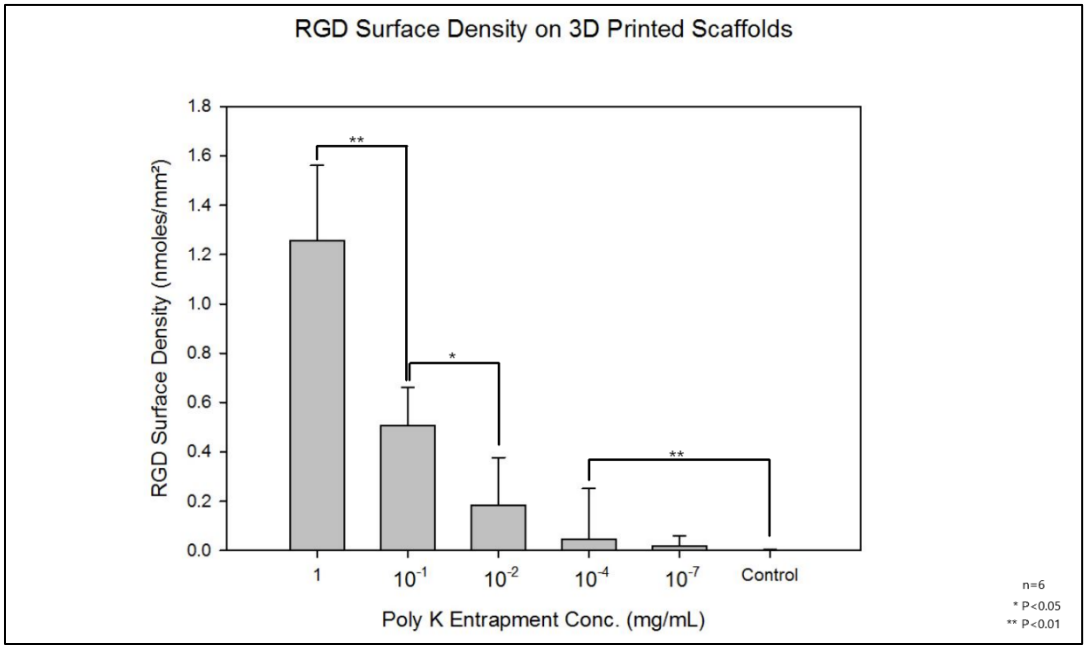

Figure 7**: RGD Amine-Coupling onto 3D printed PLLA scaffolds (n=6). Trends are similar to 2D films.**

Figure 7 showcases the same RGD amine-coupling reaction shown in Figure 6 through 2D films now on 3D scaffolds. The overall functionalization process was the same which utilized a functionalized PLLA surface that was modified with SPDP and RGD. Similarly, the levels of reacted RGD varies from 1 mg/mL to 10^{-7} mg/mL and a control without entrapped Poly K. There

are significant differences between all of 1, 10^{-1} mg/mL, 10^{-2} and 10^{-4} mg/mL; however, there is now a significant difference for the 10^{-7} mg/mL functionalized scaffolds and control unlike to the observations of the functionalized 2D films in Figure 6. The same trend and possible physisorption dynamic can be seen in these 3D scaffolds as were seen in the 2D films. Similarly to the 2D films, the average RGD surface density will be used to signify the Poly K entrapment and the subsequent RGD functionalization. Ultimately, there seems to be another trend of increasing Poly K entrapment and functionalized RGD on the surface of the 3D scaffold. This may also be due to diffusion limitations of 3D printed scaffold when compared to the 2D PLLA film and their ability to absorb Poly K onto the surface of the polymer.

3.4 T-Cell Attachment with 2D

3.4.1 2D T-Cell Attachment (Assay)

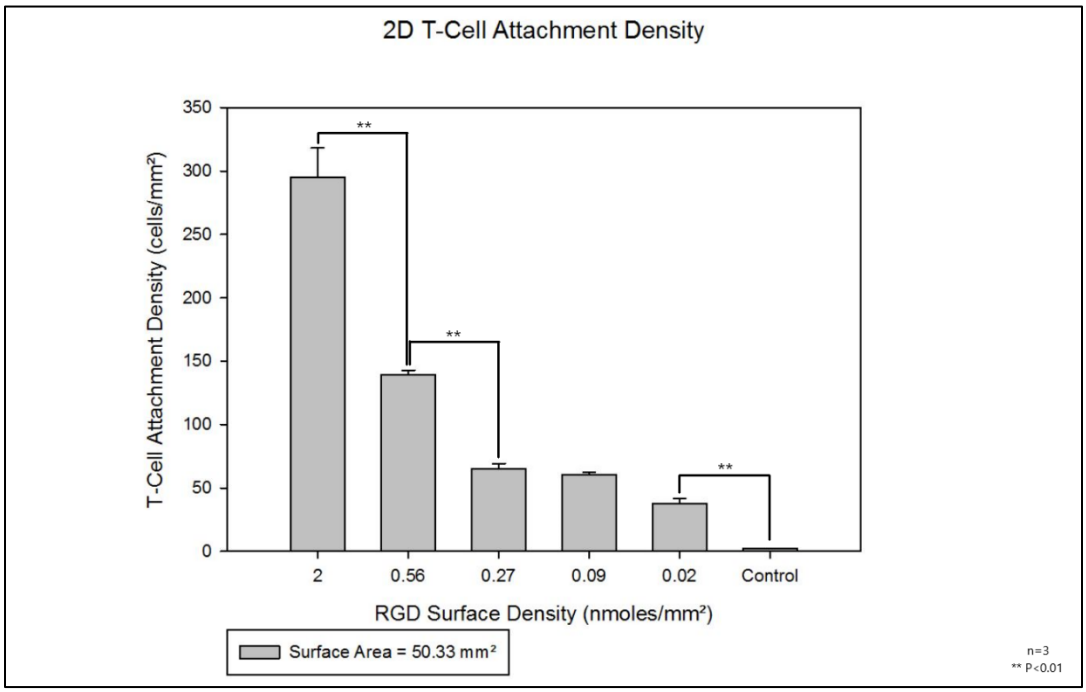

Figure 8: **2D T-Cell attachment density onto 2D PLLA films to test peptide adhesion properties (n=3). Trends do seem to match the RGD density seen on the films. Cells attachment seems to be affected by the RGD peptides.**

CD8+ T-cells represent a part of the immune system that interacts with cancer and as such their cancerous exosomes as well. Out of the possible immunological components tied with immune response, like CD8+ and CD4+ T-cells, macrophages, Regulatory T-cells, and dendritic cells for example, CD8+ T-cells represent the common-place cytotoxic response implemented by the body. To create a proof-of-concept system a decrease in overall system complexity needs to first be implemented. As the CD4+ T-cell response is produced by an intermediary antigen presentation, and the fact that Regulatory T-Cells can present both CD4 and CD8, the CD8+ T-cells represent an earlier step for the elimination of neoplastic cells and thus warrant the initial exploration in a 3D macroscale system [161]. Although T-Cells are also suspension-based, immobilization and proximity are necessary for the experimental design.

The RGD functionalized PLLA films were used to test T-cell attachment due to commonplace binding motif of RGD for T-cells. Due to cytokine production in activated T-cells, these tests had an additional benefit that IL-2 production could relate indirectly to the activation of a T-cells when attached to the RGD functionalized surfaces. T-cells were cultured with the RGD functionalized films and then stimulated to test for their IL-2 cytokine production. RGD functionalized films using Poly K entrapment solutions and their respective RGD surface density of 2.00±0.56 to 0.02±0.28 nmoles/mm^2 and control were used for the T-Cell attachment tests. T-cell attachment as reported in Figure 8 seems to agree with the RGD surface density results presented in Figure 6 where RGD surface density present on the surface of the film showed significant differences between 10^{-1} and 10^{-2} mg/mL Poly K entrapment solutions used. This seems to corroborate the RGD densities seen in the 2D films in Figure 6. 1 mg/mL of poly K entrapment and its respective 2.00±0.56 nmoles/mm^2 RGD density yielded 295±23 cells/mm^2,

0.56±0.17 cells/mm^2 yielding 140±3 cells/mm^2 and 0.27±0.43 nmoles/mm^2 yielding 65±4 cells/mm^2 with no significant difference between 0.27±0.43, 0.09±0.33, and 0.02±0.28 nmoles/mm^2. The projected RGD surface density presented on the surface of the 2D films in Figure 6 present a linear trend of T-cell attachment density with RGD functionalized films which is that larger amounts of surface RGD led to larger amounts of attached T-cell density. Although for the first time we attached T-cells onto a synthetic polymer material, this response of T-cell attachment on RGD a functionalized surface was expected as a previous group attached T-cells onto the surface of a PEG-RGDS plate hydrogel and had successful attachment [162]. The attachment density and material density and composition were not provided to the extent as provided in our study, but the attachment validity was corroborated.

3.4.2 2D T-Cell Spreading (Phalloidin)

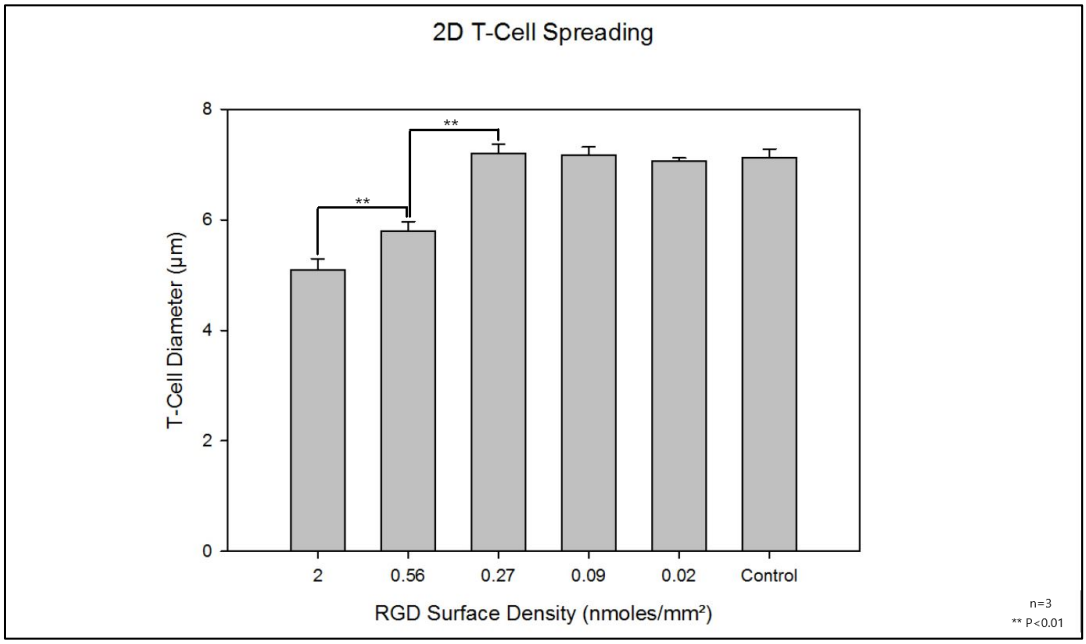

Figure 9: **T-Cell spreading as determined from a phalloidin stain on the plasma membrane actin of attached T-cells (n=3). Higher RGD surface densities seem to cause the T-cells to increase their attachment density and decrease their diameters, where normal physiological diameters are between 7 – 7.5 µm.**

An unexpected result was observed during analysis of the initial T-cell attachment on 2D modified films. There seemed to exist a diameter difference between attached T-cells at higher RGD surface densities compared to lower surface densities. An initial assessment was done via microscope observations and determined that there was a discrepancy in cell spreading based on the RGD functionalization of the Poly K entrapment solutions. As a reference, mesenchymal stem cells tend to have increased cell spreading as surface functionalization concentrations increase. A phalloidin assay was performed to stain the actin present in the cell membrane of the T-cells, and the diameters obtained from the stain can be seen in Figure 9. Diameters of the attached T-cells ranged from 7.2±.2 to 5.1±.3 μm with RGD surface densities of 0.02±0.28 and 2.00±0.56 nmoles/mm^2. A diameter of almost 5 μm diameter was produced by a RGD surface density of 2.00±0.56 nmoles/mm^2. The diameters did not regain a typical physiological diameter of 7.5 μm until 10^{-2} mg/mL poly K seeding. The increase of T-cell attachment can be seen in Figure 10, where the higher RGD surface densities have increased attachment density. The lower cell spreading at higher RGD densities seemed to be due to an overabundance of attached T-cells on the 2D film which can be related to the approximated RGD surface density present on the surface of films, similar to the results in Figure 6. This could also be due to the ability of T-cells in vivo to squeeze through diameters smaller than average T-cells size based on physiological conditions when responding to immune signals [163]. These results led to an upper limit of 10^{-2} mg/mL of poly K entrapment concentrations for subsequent trials and 3D testing to accommodate for decreased cell spreading and to retain the physiological norm for T-cells.

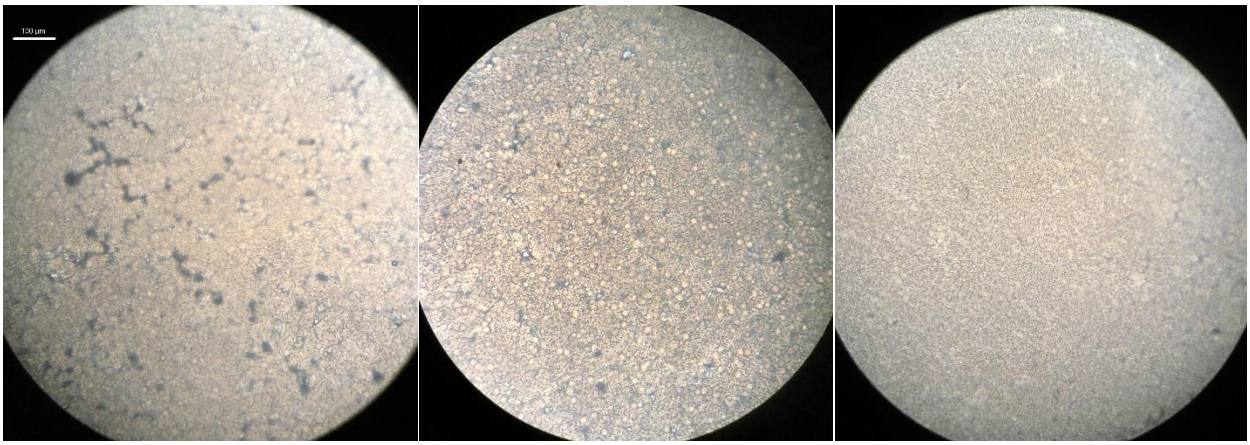

Figure 10**: Images of T-cells on 2D PLLA films of Poly K Seeding concentrations of 10^{-7} mg/mL, 10^{-2} mg/mL, and 10^{-1} mg/mL and their respective RGD surface densities of 0.02±28, 0.26±43, and 0.56±0.17 nmoles/mm2. T-cell diameter can be seen to continually decrease as the density of attached cells also increases.**

3.5 T-Cell Attachment with 3D

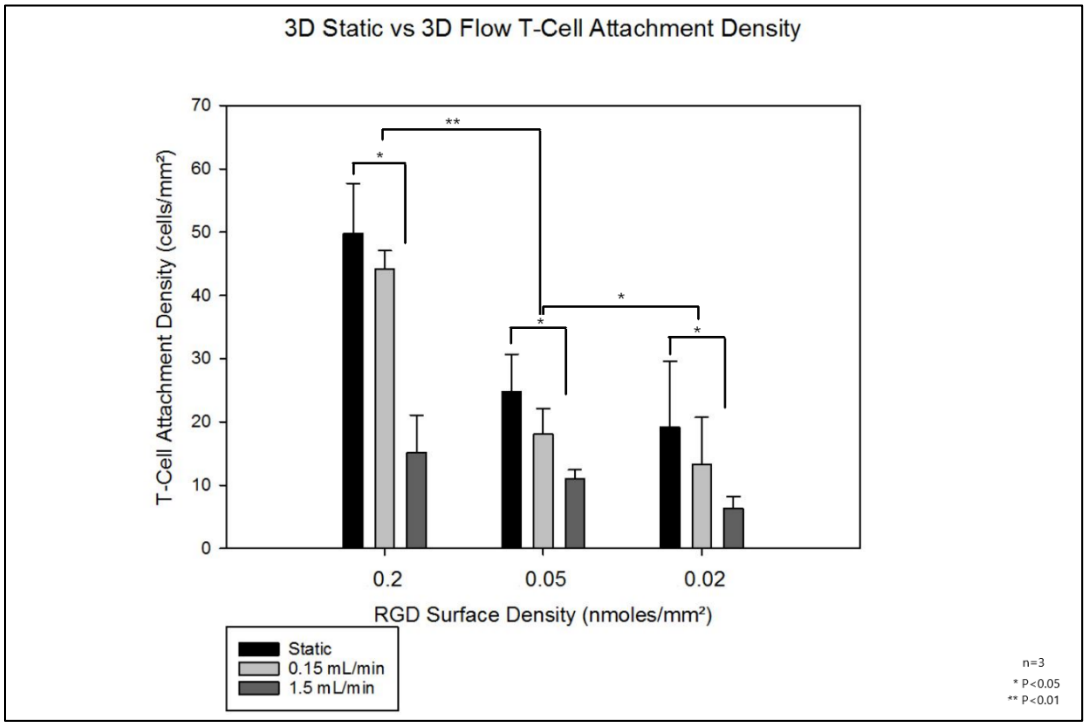

Figure 11**: Comparison of flow in the 3D flow perfusion bioreactor of attached T-cells onto the 3D printed scaffolds (n=3). Flow rates range from 0.15 mL/min to 1.5 mL/min, or superficial velocities of 1.2±0.5 mm/min to 12.4±0.1 mm/min through each scaffold, based on pump specifics. The static 3D attachment is provided as a reference.**

Static 3D cultures were first tested to determine the viability of T-cell attachment onto a 3D printed and RGD functionalized scaffold as well as to determine the starting T-cell concentrations and cell numbers prior to testing under flow conditions. Static conditions do not

represent the dynamic environments seen in vivo, and as such the cells attached during static testing may also not represent the cell numbers attached in dynamic environments. As both cells and scaffolds are subjected to flow, the strength of the binding motif for the cell attachment is tested against the shear forces generated by the flow. The functionalized scaffolds and their cell attachment must be able to withstand the dynamic conditions of the system without being removed to be able to withstand further tests under those same conditions. Figure 11 shows the attachment of T-cell on RGD functionalized 3D scaffolds under both static conditions and flow, with the lowest and highest bioreactor flow conditions being 0.15 mL/min and 1.5 mL/min. The effective superficial velocity through each scaffold ranges from 1.2±0.5 mm/min to 12.4±0.1 mm/min. A RGD surface density was selected for these experiments to avoid cell spreading concerns observed in Figure 9 and to optimize cell retention. Lower surface densities have also been used to identify effects on binding motif strength of the RGD surface densities on attached T-cells. Control groups with no RGD have not been used because in preliminary experiments have shown non-existent T-cell attachment. Static conditions began with T-cell numbers as high as 50±8 cells/mm^2 for the RGD surface density of 0.27±0.43 nmoles/mm^2 to 13.3±7.4 cells/mm^2 for 0.02±0.28 nmoles/mm^2.

Figure 11 shows that T-cells remained on the 3D printed scaffold through over 4 hours of continuous flow even with the highest flow conditions of 1.5 mL/min. There is a significant difference between static 3D functionalized scaffolds and their dynamic flow counterparts; however, the percentages between each flow condition differ. For the highest RGD surface density compared to the static T-cell attachment density 0.15 mL/min retained 89±11% T-cells and 1.5 mL/min retained 30±8% T-cells. For the lowest RGD surface density of 0.27±0.43 nmoles/mm^2, the static seeding related to a drop in T-Cell attachment density to 69±13% and

19±12% for the 0.15 mL/min and 1.5 mL/min respectively. The drop observed in the T-cell attachment density due to flow was much more moderate. The shear rate through both flows were, respectively, 500 s^{-1} and 50 s^{-1}, with estimated shear forces of 0.04 dynes/cm^2 and 0.007 dynes/cm^2. It seems that the shear stress and shear rates disproportionately impacted cell adhesion, as there was an 80% increase in the shear experienced by the cells compared to the, on average, 50% drop in cell density between the 1.5 and 0.15 mL/min results. Overall, across all 3 RGD densities tested, the t-cell attachment density from the surface was around 80±10% while the 1.5 mL/min was much more significant as 33±18%, and as such when we did exosome testing the 0.15 mL/min was selected. The 0.27±0.43 nmoles/mm^2 and 0.15 mL/min conditions were selected to optimize cell attachment and number. Cell density seems to play a role in cell retention under flow conditions as higher RGD functionalization yielded larger cell retentions under both the high and low dynamic flow conditions. It may be possible that larger RGD surface densities may provide stronger adhesion properties for attached T-cells compared to surfaces with lower nmoles of RGD. This has been the first time that T-cells have been immobilized within 3D flow, as previous studies have been done in 3D suspension culture systems, so the comparisons from historical data do not elucidate any trends for the behaviors under flow.

3.6 Exosome Co-Culture

3.6.1 2D Co-Culture

Cancerous exosomes have been shown to interact with the immune system which means that they interact with T-cells. Common changes resulting from T-cell interactions involve the production of cytokines. When T-cells interact with a system, there are specific cytokine productions that indicate response from proliferation and cell-signaling, among others, and these

cytokines and their productions can be related to the activation of T-cells. The cytokine production of IL-2, which is a common cytokine produced from activated T-cells, can be used to relate both the activation and exposure of exosomes with attached T-cells. The cytokines produced are typically related to the stimulant used with the T-cells, where PMA being a common chemical stimulant which produces IL-2 and relates to proliferation. As exosomes typically outnumber cells on an order of magnitude of 10^3, varied ratios of T-cells to exosomes were used to judge the impact of exosomes concentrations on the silencing of T-cells and their immune response [164]. Two separate exosomes from different cancerous cell lines were used to compare the impact of exosomes derived from different systems. As stated in the methods, H1299 is a human non-small cell lung carcinoma cell line and A549 is an adenocarcinomic human alveolar basal epithelial cell line.

Figure 12 shows the modified 2D PLLA film individually co-cultured with exosomes from both H1299 and A549 cancerous cell lines. Immediately, there is an observable difference from the IL-2 production of T-cells cultured on 2D PLLA films without exosomes and their exosome co-culture counterparts. Both exosomes from H1299 and A549 seem to impact the IL-2 production and deactivation of T-cells based on the lowered IL-2 production as the ratio of exosomes to T-cells increase. Higher concentration of exosomes results in a lower IL-2 production from T-cells attached onto the modified films. 1:10 and 1:20 T-cell to exosome ratio resulted in no detectable IL-2 production. On the other hand, IL-2 production was detected from 1:1 and 1:5 T-cell and exosome ratios resulting in 2900±300 and 600±50 pg/mL of IL-2 for H1299 and 3500±700 and 800±300 pg/mL of IL-2 for A549, respectively. The overall IL-2 response when comparing the H1299 and A549 exosomes show that there are higher IL-2 productions in the A549 exosomes

which can be said to lead to a lower silencing of the T-cells when compared to H1299 exosomes; however, there is not a significant enough of a difference between the two populations to make a substantiated claim. Even at the 1:1 ratio there is a limited silencing compared to the baseline shown above the figure, but the negligible IL-2 production starting at ratios of 1:10 can be used to justify a silencing of the T-cells and their immune response when in contact with cancerous exosomes on 2D films. It should be noted that the 2D films were cultured for 4-hours in a static condition which forced continual interactions between the exosomes and the attached T-cells. Now, multiple studies have cultured T-cells, however not immobilized, with cancer exosomes from many differing cell lines and cancer patients like melanoma, breast, neck and head, and lung cancers [165, 166]. and showed that their respective cancerous exosomes had immunosuppressive properties. Although these results were expected as both exosomes were from cell lines from separate types of cancer, it can be said that the cancer exosomes that were cultured provided some to complete immunosuppressive properties in 2D static cultures.

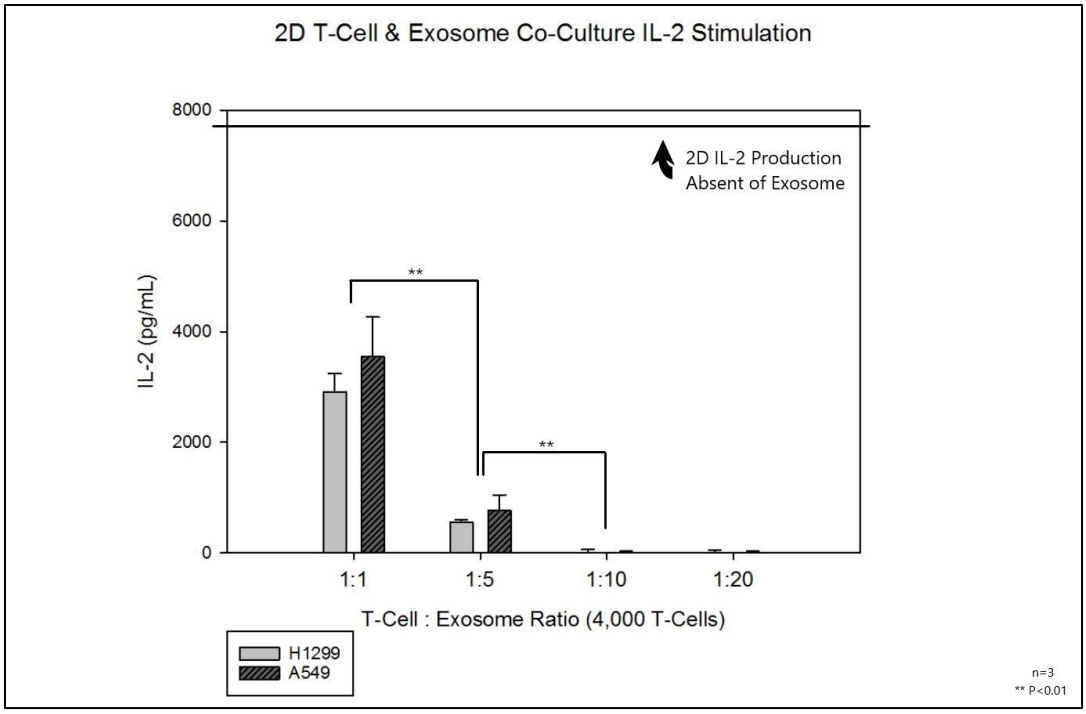

Figure 12**: 2D PLLA film co-culture of CD8+ T-cells and exosomes from H1299 and A549 cell lines (n=3). This experiment denotes the response to the presence of exosomes when attached to the same material as used in 3D scaffolds, but without flow.**

3.6.2 3D Static Co-Culture

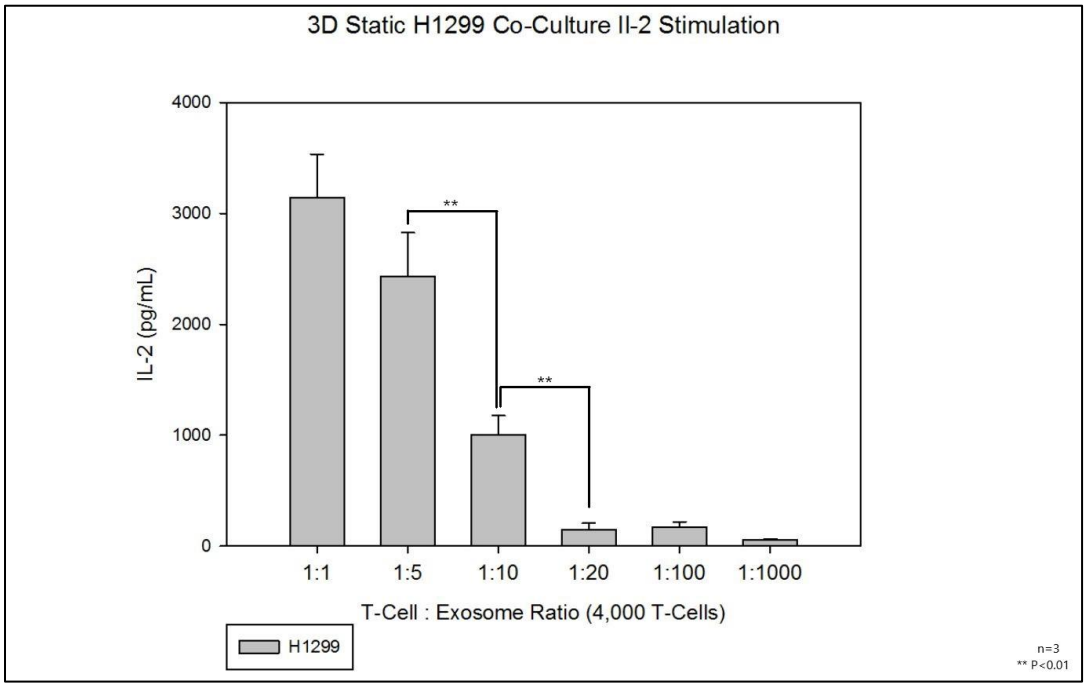

Figure 13**: Co-culture of H1299 exosomes with CD8+ T-cells on the 3D printed scaffolds (n=3). The IL-2 production from the T-cell stimulation can be seen to decrease as the exosome ratio increases.**

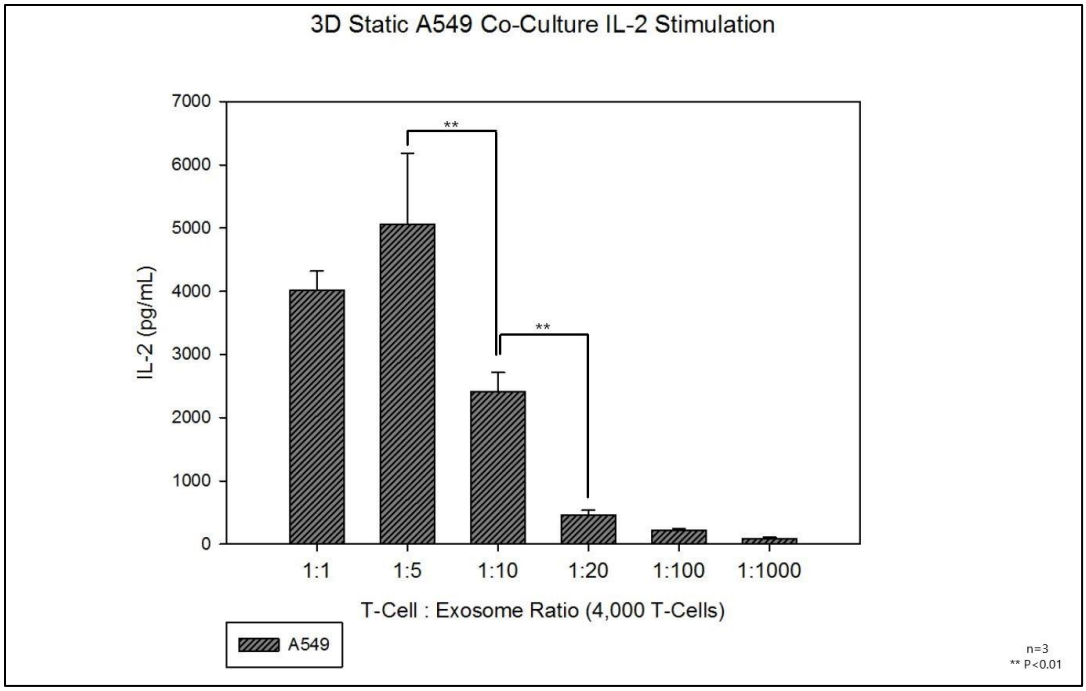

Figure 14**: Co-culture of A549 exosomes with CD8+ T-cells on the 3D printed scaffolds (n=3). The IL-2 production, similar to the H1299 exosomes (Figure 13), showed an overall decreasing trend with increasing exosome ratio, although the 1:5 ratio 1:5 is higher but shows no significance from 1:1.**

Figures 13 and 14 showcase the same static exosomes co-culture with attached T-cells, but now using 3D modified scaffolds. The 3D static conditions for both H1299 and A549 exosome co-cultures present similar results to their modified 2D counterparts, but the IL-2 production seems to be larger compared to the 2D films. Since 4,000 T-cells were attached using the RGD binding motif, a similar result should be seen from the 2D and 3D comparison; however, the slight deviation may be due to diffusion limitations present in the 3D structure. Again, exosomes from the H1299 cell line seem to produce a lower IL-2 response from the static 3D scaffolds compared to the A549 cell line. Although there are discrepancies shown in A549 on the 1:5 ratio, the overall trend remains similar and the highest concentrations of exosome co-culture result in decreasing levels of IL-2 production which relate to a silencing of the T-cells.

3.6.3 3D Flow Co-Culture

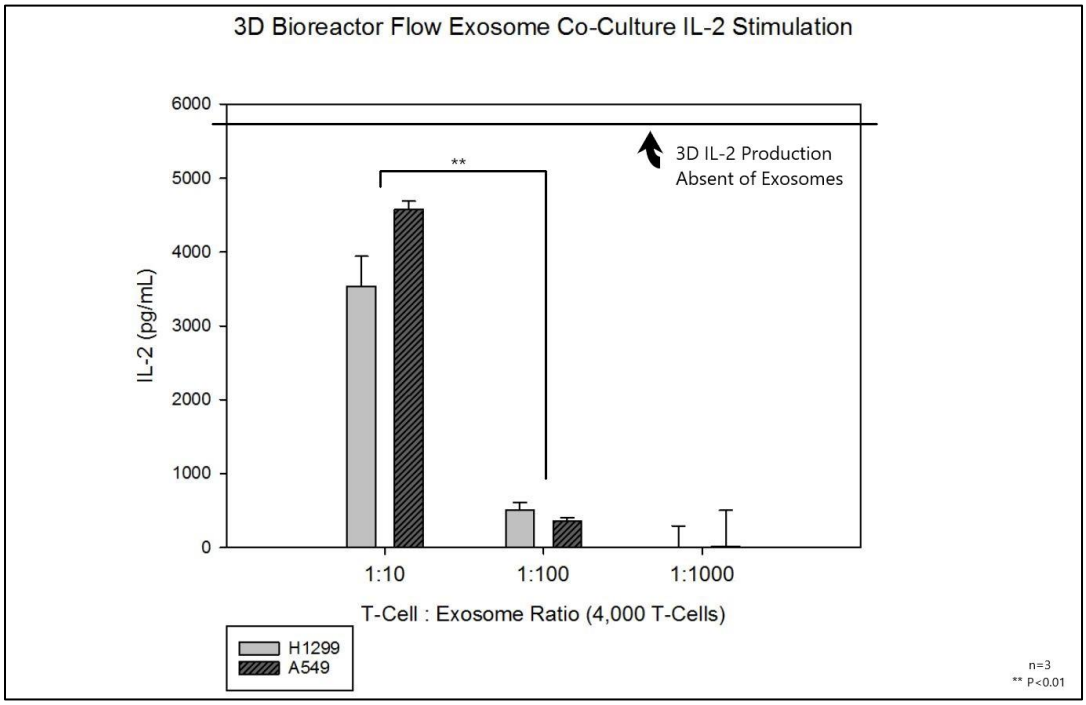

Figure 15**: Co-culture of CD8+ T-cells on 3D printed scaffolds with both H1299 and A549 exosomes (n=3). Only 3 concentrations were used. Lower exosome ratios yielded similar results to 3D static co-culture with higher having lower responses.**

Exosome co-culture under dynamic conditions like flow more accurately replicate physiological conditions. IL-2 productions can be compared to their static 3D counterparts to determine the overall efficacy of cancerous exosomes on the silencing of immune cells. Potential diffusion limitations seen in static conditions, like comparing the baseline IL-2 production from both 2D static cultures to the 3D baseline showing lower overall IL-2 values, should be alleviated using flow. The responses from the PMA stimulation in 3D flow perfusion resulted in significantly higher IL-2 production from the same respective concentration of circulating exosomes as seen in Figure 15. Again, from Figure 12, 1:10 ratios resulted in IL-2 productions of 2900±300 and 3500±700 pg/mL for H1299 and A549 up to 3500±400 and 4600±500 pg/mL, respectively, for the 1:10 3D counterpart. As seen throughout both 2D and 3D exosomes co-cultures, an increased exosome ratio resulted in a decreased IL-2 production from attached T-cells. Although responses

were present in all static 3D culture exosome concentrations, the flow perfusion culture seems to entirely silence the response of the T-cells with highest concentrations of exosomes of 1:1000. This may be due to the physiological concentration of exosomes and their relative overabundance in the body compared to other cells with an estimated relation of overall a billion exosomes per million of cells [164]. As this was also the first 3D flow exosome co-culture, comparisons with historical data are not present. Although the responses seem significantly larger compared to previous results, it must be considered that the working volumes of the bioreactor flow conditions could relate differently to the static conditions. The static conditions, for both 2D films and 3D scaffolds, used 1 mL of stimulant solution while each bioreactor cassette used 5 mL of working volume. These discrepancies have been accounted for as the exosome ratio was per mL of fluid used so, for example, the 1:10 ratio are comparable in both 2D and 3D static and 3D flow.

The 3D comparison shows that the overall IL-2 production decrease is far lower than those compared to the 2D static cultures. Although the 1:10 exosome ratio in the 2D cultures produced IL-2 levels that were almost negligible, the 3D flow perfusion exosome co-cultures produced IL-2 responses that were higher than the lowest exosome ratio in the 2D cultures. Even at 10 times the exosome ratio the IL-2 response in the 3D cultures were not negligible. A suppression of the IL-2 production was not detected until 100 times that of the 2D static cultures with a 1:1000 exosome ratio. In a cancer exosome study, the blood of melanoma patients was collected, and within each mL of blood collected, the exosome profile was examined. It was found that of the 10^{10} exosomes in the blood found, the total percentage of cancer exosomes ranged from 20% to 70% within these patients [167]. This stark difference in circulating exosomes is the precise environment that 2D cultures do that recapitulate. As said earlier, the number of cells in blood

typically range from 10^6 to 10^7 cells/mL, and this difference in relative concentration has a noticeable impact on exosome co-cultures, as seen in the difference between IL-2 production from Figure 12 and Figure 15. The overall number of white blood cells within the human body is approximately 10^9 for the 5 L of blood, which places an exosome-white blood cell ratio in the body as 1:5000 and similar magnitude to the levels tested. The 3D flow comparison effectively demonstrates that there seems to be a dose response with cancerous exosomes and their impact on immune cells. If the time scale of exosome T-cell interactions were known, the velocity within the porosity could be an important parameter for the system.

The implications of these findings relate heavily to the 3D in vitro system providing better tailored systems to replicate and recapitulate in vivo systems. As the 3D system seems to differ heavily from 2D responses, these systems can be developed to better test patient-specific aspects, like mass screening for potential therapeutics. A more complex 3D system can even translate to identifying means to reduce the impact of cancerous exosomes on their influence of immune cells and the immune system.

4. CONCLUSION

Analysis of the 3D flow perfusion system yielded results that show the translation of both T-cells and exosomal co-culture from modified 2D PLLA films to 3D printed scaffolds with surface modifications. Surface modification techniques from previous works were redone to test their validity and effectiveness since T-cells bind strongly to the RGD [159, 160]. RGD peptide incorporation translated well from 2D 8 mm films to 3D printed scaffolds, with RGD surface densities peptides from the highest and lowest seeding concentrations ranging from 2.00±0.58 nmoles/mm2 for 1 mg/mL to 0.02±0.28 nmoles/mm2 for 10-7 mg/mL. T-cell attachment was a foundation project goal as immobilized T-cells were not common in literature. The use of PMA to produce IL-2 responses was successful and presented two benefits: (1) provided a means to detect T-cell activation and (2) provided an indirect, non-destructive method of immobilized T-cell quantification. Although attachment was successful, there was an unexpected occurrence of decreased cell spreading from oversaturation of T-cells reducing their diameters below physiological occurrences which was accommodated in subsequent testing.

The two next crucial goals for the project were 3D flow and exosomal co-culture. 3D flow showed interesting results, but most importantly showed that T-cell retention was evident for even the highest flowrates of 1.5 mL/min with around 33±18% cells after 4 hours of flow. The last step for this project was testing exosomal co-culture and its impact on immunosuppression. Exosomes provided from both H1299 and A549 cell lines were effective in reducing IL-2 production, but the overall IL-2 production was highest in static 3D constructs with 2D films having IL-2 production as low as 85±5 pg/mL of IL-2 compared to 2500±600 and 8300±1000 pg/mL for the two static 3D conditions. Interestingly, the overall IL-2 production was similar

between the 1:20 3D static culture to 1:100 flow perfusion ratios due to the 5-fold increase of the bioreactors working volumes compared to static testing.

Ultimately, the goal of the project was to test the impacts of exosomal co-culture on T-cell and immunosuppression. Our results found that surface modification was successful in immobilizing T-cells to both 2D films and to 3D printed scaffolds. Although some T-cells were lost during bioreactor flow testing, up to 80±10% of the T-cells were retained at the lowest flow rate. Exosomal co-culture showed that there is a drop in IL-2 production as the ratio of T-cells to exosome increases. This IL-2 decrease based on our results show that there is an immunosuppressive interaction with the immobilized T-cells and the circulating exosomes in the system and that these interactions can be reproduced in our 3D flow perfusion system. Overall, the experimentation has added useful data for the next steps of an overarching cancer modeling system where T-cells and exosomes can be part of a more complex system.

5. FUTURE DIRECTIONS

The results of this study showed the capacity to incorporate a complex bioreactor system with both T-cells and exosomes concurrently. Although the results were positive, there are places to improve and next steps to take. To begin, the PMA stimulation should be tested over a range of concentrations and times to determine an effective dose that optimizes IL-2 production for the number of T-cells present as well as optimizes cost for the stimulation. Alongside the PMA stimulation, there exists another optimization with bioreactor flow rates. Due to the fact that there is a decreasing retention with bioreactor flow rate, testing should be done to not only optimize T-cell retention against flow, but also test flow characteristics and properties on T-cell dynamics and exosomal effects. As for the exosome testing, co-culture and stimulation times need to be optimized for the characterization profiles. As exosome concentrations are magnitudes higher than cells, incorporating different exosome ratios to test impacts can be impactful as well.

The future directions for the project and in vitro 3D system have huge potential. Since T-cells and exosomes are now possible to co-culture, the system can now be extended towards more complex areas. The incorporation of pharmaceuticals and other cancer therapeutics alongside the fully developed system can test whether their effects can impact T-cell cytokine productions. Treatments can even be tested that reduce only cancerous exosome secretion and leave healthy cells unimpacted. On the same note, other cytokine concentrations can be tested and measured to test their effects with not only exosomes, but other environmental conditions. The bioreactor system set-up allows for a potential for an even deeper cancer environment to develop with upstream and downstream cultures to test not only their influence on each other, but also how they interact with external system components like drugs and exosomes.

6. REFERENCES

[1] C. Global Burden of Disease Cancer, C. Fitzmaurice, C. Allen, R.M. Barber, L. Barregard, e. al., Global, Regional, and National Cancer Incidence, Mortality, Years of Life Lost, Years Lived With Disability, and Disability-Adjusted Life-years for 32 Cancer Groups, 1990 to 2015: A Systematic Analysis for the Global Burden of Disease Study, JAMA Oncol, 3 (2017) 524-548.
[2] B. Stewart, World Cacner Report, World Health Organization, (2014).
[3] M.O. Palumbo, P. Kavan, W.H. Miller, Jr., L. Panasci, S. Assouline, N. Johnson, V. Cohen, F. Patenaude, M. Pollak, R.T. Jagoe, G. Batist, Systemic cancer therapy: achievements and challenges that lie ahead, Front Pharmacol, 4 (2013) 57.
[4] B.P. Cabral, M. da Graca Derengowski Fonseca, F.B. Mota, The recent landscape of cancer research worldwide: a bibliometric and network analysis, Oncotarget, 9 (2018) 30474-30484.
[5] Y. Sun, W. Zheng, Z. Guo, Q. Ju, L. Zhu, J. Gao, L. Zhou, F. Liu, Y. Xu, Q. Zhan, Z. Zhou, W. Sun, X. Zhao, A novel TP53 pathway influences the HGS-mediated exosome formation in colorectal cancer, Sci Rep, 6 (2016) 28083.
[6] J.H. Hurley, G. Odorizzi, Get on the exosome bus with ALIX, Nat Cell Biol, 14 (2012) 654-655.
[7] L. Urbanelli, A. Magini, S. Buratta, A. Brozzi, K. Sagini, A. Polchi, B. Tancini, C. Emiliani, Signaling pathways in exosomes biogenesis, secretion and fate, Genes (Basel), 4 (2013) 152-170.
[8] M. Yanez-Mo, P.R. Siljander, Z. Andreu, A.B. Zavec, F.E. Borras, E.I. Buzas, K. Buzas, E. Casal, F. Cappello, J. Carvalho, E. Colas, A. Cordeiro-da Silva, S. Fais, J.M. Falcon-Perez, I.M. Ghobrial, B. Giebel, M. Gimona, M. Graner, I. Gursel, M. Gursel, N.H. Heegaard, A. Hendrix, P. Kierulf, K. Kokubun, M. Kosanovic, V. Kralj-Iglic, E.M. Kramer-Albers, S. Laitinen, C. Lasser, T. Lener, E. Ligeti, A. Line, G. Lipps, A. Llorente, J. Lotvall, M. Mancek-Keber, A. Marcilla, M. Mittelbrunn, I. Nazarenko, E.N. Nolte-'t Hoen, T.A. Nyman, L. O'Driscoll, M. Olivan, C. Oliveira, E. Pallinger, H.A. Del Portillo, J. Reventos, M. Rigau, E. Rohde, M. Sammar, F. Sanchez-Madrid, N. Santarem, K. Schallmoser, M.S. Ostenfeld, W. Stoorvogel, R. Stukelj, S.G. Van der Grein, M.H. Vasconcelos, M.H. Wauben, O. De Wever, Biological properties of extracellular vesicles and their physiological functions, J Extracell Vesicles, 4 (2015) 27066.
[9] M. Gonzalez-Begne, B. Lu, X. Han, F.K. Hagen, A.R. Hand, J.E. Melvin, J.R. Yates, Proteomic analysis of human parotid gland exosomes by multidimensional protein identification technology (MudPIT), J Proteome Res, 8 (2009) 1304-1314.
[10] J.M. Garcia, V. Garcia, C. Pena, G. Dominguez, J. Silva, R. Diaz, P. Espinosa, M.J. Citores, M. Collado, F. Bonilla, Extracellular plasma RNA from colon cancer patients is confined in a vesicle-like structure and is mRNA-enriched, RNA, 14 (2008) 1424-1432.
[11] J.W. Dear, J.M. Street, M.A. Bailey, Urinary exosomes: a reservoir for biomarker discovery and potential mediators of intrarenal signalling, Proteomics, 13 (2013) 1572-1580.
[12] M. Record, C. Subra, S. Silvente-Poirot, M. Poirot, Exosomes as intercellular signalosomes and pharmacological effectors, Biochem Pharmacol, 81 (2011) 1171-1182.
[13] F. Raimondo, L. Morosi, C. Chinello, F. Magni, M. Pitto, Advances in membranous vesicle and exosome proteomics improving biological understanding and biomarker discovery, Proteomics, 11 (2011) 709-720.
[14] L. Balaj, R. Lessard, L. Dai, Y.J. Cho, S.L. Pomeroy, X.O. Breakefield, J. Skog, Tumour microvesicles contain retrotransposon elements and amplified oncogene sequences, Nat Commun, 2 (2011) 180.

[15] D. Burger, S. Schock, C.S. Thompson, A.C. Montezano, A.M. Hakim, R.M. Touyz, Microparticles: biomarkers and beyond, Clin Sci (Lond), 124 (2013) 423-441.
[16] J. Cai, Y. Han, H. Ren, C. Chen, D. He, L. Zhou, G.M. Eisner, L.D. Asico, P.A. Jose, C. Zeng, Extracellular vesicle-mediated transfer of donor genomic DNA to recipient cells is a novel mechanism for genetic influence between cells, J Mol Cell Biol, 5 (2013) 227-238.
[17] B.K. Thakur, H. Zhang, A. Becker, I. Matei, Y. Huang, B. Costa-Silva, Y. Zheng, A. Hoshino, H. Brazier, J. Xiang, C. Williams, R. Rodriguez-Barrueco, J.M. Silva, W. Zhang, S. Hearn, O. Elemento, N. Paknejad, K. Manova-Todorova, K. Welte, J. Bromberg, H. Peinado, D. Lyden, Double-stranded DNA in exosomes: a novel biomarker in cancer detection, Cell Res, 24 (2014) 766-769.
[18] D. Garcia-Olmo, D.C. Garcia-Olmo, J. Ontanon, E. Martinez, M. Vallejo, Tumor DNA circulating in the plasma might play a role in metastasis. The hypothesis of the genometastasis, Histol Histopathol, 14 (1999) 1159-1164.
[19] M. Abdouh, S. Zhou, V. Arena, M. Arena, A. Lazaris, R. Onerheim, P. Metrakos, G.O. Arena, Transfer of malignant trait to immortalized human cells following exposure to human cancer serum, J Exp Clin Cancer Res, 33 (2014) 86.
[20] Z.Y. Abd Elmageed, Y. Yang, R. Thomas, M. Ranjan, D. Mondal, K. Moroz, Z. Fang, B.M. Rezk, K. Moparty, S.C. Sikka, O. Sartor, A.B. Abdel-Mageed, Neoplastic reprogramming of patient-derived adipose stem cells by prostate cancer cell-associated exosomes, Stem Cells, 32 (2014) 983-997.
[21] D. Hamam, M. Abdouh, Z.H. Gao, V. Arena, M. Arena, G.O. Arena, Transfer of malignant trait to BRCA1 deficient human fibroblasts following exposure to serum of cancer patients, J Exp Clin Cancer Res, 35 (2016) 80.
[22] C.V. Harding, J.E. Heuser, P.D. Stahl, Exosomes: looking back three decades and into the future, J Cell Biol, 200 (2013) 367-371.
[23] S.A. Melo, H. Sugimoto, J.T. O'Connell, N. Kato, A. Villanueva, A. Vidal, L. Qiu, E. Vitkin, L.T. Perelman, C.A. Melo, A. Lucci, C. Ivan, G.A. Calin, R. Kalluri, Cancer exosomes perform cell-independent microRNA biogenesis and promote tumorigenesis, Cancer Cell, 26 (2014) 707-721.
[24] A. Riches, E. Campbell, E. Borger, S. Powis, Regulation of exosome release from mammary epithelial and breast cancer cells - a new regulatory pathway, Eur J Cancer, 50 (2014) 1025-1034.
[25] M.T. Le, P. Hamar, C. Guo, E. Basar, R. Perdigao-Henriques, L. Balaj, J. Lieberman, miR-200-containing extracellular vesicles promote breast cancer cell metastasis, J Clin Invest, 124 (2014) 5109-5128.
[26] Y. Mosesson, G.B. Mills, Y. Yarden, Derailed endocytosis: an emerging feature of cancer, Nat Rev Cancer, 8 (2008) 835-850.
[27] I. Nazarenko, S. Rana, A. Baumann, J. McAlear, A. Hellwig, M. Trendelenburg, G. Lochnit, K.T. Preissner, M. Zoller, Cell surface tetraspanin Tspan8 contributes to molecular pathways of exosome-induced endothelial cell activation, Cancer Res, 70 (2010) 1668-1678.
[28] L. Alvarez-Erviti, Y. Seow, H. Yin, C. Betts, S. Lakhal, M.J. Wood, Delivery of siRNA to the mouse brain by systemic injection of targeted exosomes, Nat Biotechnol, 29 (2011) 341-345.
[29] D. Sousa, R.T. Lima, M.H. Vasconcelos, Intercellular Transfer of Cancer Drug Resistance Traits by Extracellular Vesicles, Trends Mol Med, 21 (2015) 595-608.

[30] G. Taraboletti, S. D'Ascenzo, I. Giusti, D. Marchetti, P. Borsotti, D. Millimaggi, R. Giavazzi, A. Pavan, V. Dolo, Bioavailability of VEGF in tumor-shed vesicles depends on vesicle burst induced by acidic pH, Neoplasia, 8 (2006) 96-103.
[31] W.X. Chen, X.M. Liu, M.M. Lv, L. Chen, J.H. Zhao, S.L. Zhong, M.H. Ji, Q. Hu, Z. Luo, J.Z. Wu, J.H. Tang, Exosomes from drug-resistant breast cancer cells transmit chemoresistance by a horizontal transfer of microRNAs, PLoS One, 9 (2014) e95240.
[32] M.B. Meads, R.A. Gatenby, W.S. Dalton, Environment-mediated drug resistance: a major contributor to minimal residual disease, Nat Rev Cancer, 9 (2009) 665-674.
[33] A.S. Azmi, B. Bao, F.H. Sarkar, Exosomes in cancer development, metastasis, and drug resistance: a comprehensive review, Cancer Metastasis Rev, 32 (2013) 623-642.
[34] K.G. Chen, J.C. Valencia, B. Lai, G. Zhang, J.K. Paterson, F. Rouzaud, W. Berens, S.M. Wincovitch, S.H. Garfield, R.D. Leapman, V.J. Hearing, M.M. Gottesman, Melanosomal sequestration of cytotoxic drugs contributes to the intractability of malignant melanomas, Proc Natl Acad Sci U S A, 103 (2006) 9903-9907.
[35] F. Luciani, M. Spada, A. De Milito, A. Molinari, L. Rivoltini, A. Montinaro, M. Marra, L. Lugini, M. Logozzi, F. Lozupone, C. Federici, E. Iessi, G. Parmiani, G. Arancia, F. Belardelli, S. Fais, Effect of proton pump inhibitor pretreatment on resistance of solid tumors to cytotoxic drugs, J Natl Cancer Inst, 96 (2004) 1702-1713.
[36] A.V. Bogolyubova, P.V. Belousov, Inflammatory Immune Infiltration in Human Tumors: Role in Pathogenesis and Prognostic and Diagnostic Value, Biochemistry (Mosc), 81 (2016) 1261-1273.
[37] S.I. Grivennikov, F.R. Greten, M. Karin, Immunity, inflammation, and cancer, Cell, 140 (2010) 883-899.
[38] M.D. Vesely, M.H. Kershaw, R.D. Schreiber, M.J. Smyth, Natural innate and adaptive immunity to cancer, Annu Rev Immunol, 29 (2011) 235-271.
[39] X.C. Li, M. Raghavan, Structure and function of major histocompatibility complex class I antigens, Curr Opin Organ Transplant, 15 (2010) 499-504.
[40] P.K. Anand, Exosomal membrane molecules are potent immune response modulators, Commun Integr Biol, 3 (2010) 405-408.
[41] C. Gutierrez-Vazquez, C. Villarroya-Beltri, M. Mittelbrunn, F. Sanchez-Madrid, Transfer of extracellular vesicles during immune cell-cell interactions, Immunol Rev, 251 (2013) 125-142.
[42] H.G. Zhang, W.E. Grizzle, Exosomes and cancer: a newly described pathway of immune suppression, Clin Cancer Res, 17 (2011) 959-964.
[43] G. Raposo, H.W. Nijman, W. Stoorvogel, R. Liejendekker, C.V. Harding, C.J. Melief, H.J. Geuze, B lymphocytes secrete antigen-presenting vesicles, J Exp Med, 183 (1996) 1161-1172.
[44] P.D. Robbins, A.E. Morelli, Regulation of immune responses by extracellular vesicles, Nat Rev Immunol, 14 (2014) 195-208.
[45] K.R. Qazi, U. Gehrmann, E. Domange Jordo, M.C. Karlsson, S. Gabrielsson, Antigen-loaded exosomes alone induce Th1-type memory through a B-cell-dependent mechanism, Blood, 113 (2009) 2673-2683.
[46] A.E. Morelli, A.T. Larregina, W.J. Shufesky, M.L. Sullivan, D.B. Stolz, G.D. Papworth, A.F. Zahorchak, A.J. Logar, Z. Wang, S.C. Watkins, L.D. Falo, Jr., A.W. Thomson, Endocytosis, intracellular sorting, and processing of exosomes by dendritic cells, Blood, 104 (2004) 3257-3266.
[47] A. Montecalvo, W.J. Shufesky, D.B. Stolz, M.G. Sullivan, Z. Wang, S.J. Divito, G.D. Papworth, S.C. Watkins, P.D. Robbins, A.T. Larregina, A.E. Morelli, Exosomes as a short-range

mechanism to spread alloantigen between dendritic cells during T cell allorecognition, J Immunol, 180 (2008) 3081-3090.
[48] C. Thery, L. Zitvogel, S. Amigorena, Exosomes: composition, biogenesis and function, Nat Rev Immunol, 2 (2002) 569-579.
[49] F. Andre, N.E. Schartz, M. Movassagh, C. Flament, P. Pautier, P. Morice, C. Pomel, C. Lhomme, B. Escudier, T. Le Chevalier, T. Tursz, S. Amigorena, G. Raposo, E. Angevin, L. Zitvogel, Malignant effusions and immunogenic tumour-derived exosomes, Lancet, 360 (2002) 295-305.
[50] P.P. D.H. Hsu, G. Vilaflor, A. Rivas, A. Mehta-Damani, E. Argevin, Exosomes as a tumor vaccine: enhancing potency responses by extracellular vesicles, Journal of Immunotherapy, (2003).
[51] S. Utsugi-Kobukai, H. Fujimaki, C. Hotta, M. Nakazawa, M. Minami, MHC class I-mediated exogenous antigen presentation by exosomes secreted from immature and mature bone marrow derived dendritic cells, Immunol Lett, 89 (2003) 125-131.
[52] J. Klibi, T. Niki, A. Riedel, C. Pioche-Durieu, S. Souquere, E. Rubinstein, S. Le Moulec, J. Guigay, M. Hirashima, F. Guemira, D. Adhikary, J. Mautner, P. Busson, Blood diffusion and Th1-suppressive effects of galectin-9-containing exosomes released by Epstein-Barr virus-infected nasopharyngeal carcinoma cells, Blood, 113 (2009) 1957-1966.
[53] C. Keryer-Bibens, C. Pioche-Durieu, C. Villemant, S. Souquere, N. Nishi, M. Hirashima, J. Middeldorp, P. Busson, Exosomes released by EBV-infected nasopharyngeal carcinoma cells convey the viral latent membrane protein 1 and the immunomodulatory protein galectin 9, BMC Cancer, 6 (2006) 283.
[54] V. Huber, S. Fais, M. Iero, L. Lugini, P. Canese, P. Squarcina, A. Zaccheddu, M. Colone, G. Arancia, M. Gentile, E. Seregni, R. Valenti, G. Ballabio, F. Belli, E. Leo, G. Parmiani, L. Rivoltini, Human colorectal cancer cells induce T-cell death through release of proapoptotic microvesicles: role in immune escape, Gastroenterology, 128 (2005) 1796-1804.
[55] C. Liu, S. Yu, K. Zinn, J. Wang, L. Zhang, Y. Jia, J.C. Kappes, S. Barnes, R.P. Kimberly, W.E. Grizzle, H.G. Zhang, Murine mammary carcinoma exosomes promote tumor growth by suppression of NK cell function, J Immunol, 176 (2006) 1375-1385.
[56] M. Zhou, J. Chen, L. Zhou, W. Chen, G. Ding, L. Cao, Pancreatic cancer derived exosomes regulate the expression of TLR4 in dendritic cells via miR-203, Cell Immunol, 292 (2014) 65-69.
[57] G. Ding, L. Zhou, Y. Qian, M. Fu, J. Chen, J. Chen, J. Xiang, Z. Wu, G. Jiang, L. Cao, Pancreatic cancer-derived exosomes transfer miRNAs to dendritic cells and inhibit RFXAP expression via miR-212-3p, Oncotarget, 6 (2015) 29877-29888.
[58] X. Ying, Q. Wu, X. Wu, Q. Zhu, X. Wang, L. Jiang, X. Chen, X. Wang, Epithelial ovarian cancer-secreted exosomal miR-222-3p induces polarization of tumor-associated macrophages, Oncotarget, 7 (2016) 43076-43087.
[59] N. Ludwig, B.M. Razzo, S.S. Yerneni, T.L. Whiteside, Optimization of cell culture conditions for exosome isolation using mini-size exclusion chromatography (mini-SEC), Exp Cell Res, 378 (2019) 149-157.
[60] C. Thery, K.W. Witwer, E. Aikawa, M.J. Alcaraz, e. al., Minimal information for studies of extracellular vesicles 2018 (MISEV2018): a position statement of the International Society for Extracellular Vesicles and update of the MISEV2014 guidelines, J Extracell Vesicles, 7 (2018) 1535750.

[61] M. Palviainen, H. Saari, O. Karkkainen, J. Pekkinen, S. Auriola, M. Yliperttula, M. Puhka, K. Hanhineva, P.R. Siljander, Metabolic signature of extracellular vesicles depends on the cell culture conditions, J Extracell Vesicles, 8 (2019) 1596669.
[62] D.B. Patel, K.M. Gray, Y. Santharam, T.N. Lamichhane, K.M. Stroka, S.M. Jay, Impact of cell culture parameters on production and vascularization bioactivity of mesenchymal stem cell-derived extracellular vesicles, Bioeng Transl Med, 2 (2017) 170-179.
[63] T. Umezu, S. Imanishi, K. Azuma, C. Kobayashi, S. Yoshizawa, K. Ohyashiki, J.H. Ohyashiki, Replenishing exosomes from older bone marrow stromal cells with miR-340 inhibits myeloma-related angiogenesis, Blood Adv, 1 (2017) 812-823.
[64] C. Zhang, Q. Ji, Y. Yang, Q. Li, Z. Wang, Exosome: Function and Role in Cancer Metastasis and Drug Resistance, Technol Cancer Res Treat, 17 (2018) 1533033818763450.
[65] M. Nikolic, T. Sustersic, N. Filipovic, In vitro Models and On-Chip Systems: Biomaterial Interaction Studies With Tissues Generated Using Lung Epithelial and Liver Metabolic Cell Lines, Front Bioeng Biotechnol, 6 (2018) 120.
[66] M.E. Katt, A.L. Placone, A.D. Wong, Z.S. Xu, P.C. Searson, In Vitro Tumor Models: Advantages, Disadvantages, Variables, and Selecting the Right Platform, Front Bioeng Biotechnol, 4 (2016) 12.
[67] R. Kavlock, G.T. Ankley, T. Collette, E. Francis, K. Hammerstrom, J. Fowle, H. Tilson, G. Toth, P. Schmieder, G.D. Veith, E. Weber, D.C. Wolf, D. Young, Computational toxicology: framework, partnerships, and program development. September 29-30, 2003, Research Triangle Park, North Carolina, Reprod Toxicol, 19 (2005) 265-280.
[68] K.I.a.H.R.I. Hulkower, Cell Migration and Invasion assays as tools for drug discovery, Pharmaceutics, 3 (2011).
[69] D. Wirtz, K. Konstantopoulos, P.C. Searson, The physics of cancer: the role of physical interactions and mechanical forces in metastasis, Nat Rev Cancer, 11 (2011) 512-522.
[70] D.W. Infanger, Y. Cho, B.S. Lopez, S. Mohanan, S.C. Liu, D. Gursel, J.A. Boockvar, C. Fischbach, Glioblastoma stem cells are regulated by interleukin-8 signaling in a tumoral perivascular niche, Cancer Res, 73 (2013) 7079-7089.
[71] P.A. Vidi, M.J. Bissell, S.A. Lelievre, Three-dimensional culture of human breast epithelial cells: the how and the why, Methods Mol Biol, 945 (2013) 193-219.
[72] J. Greshock, K. Nathanson, A.M. Martin, L. Zhang, G. Coukos, B.L. Weber, T.Z. Zaks, Cancer cell lines as genetic models of their parent histology: analyses based on array comparative genomic hybridization, Cancer Res, 67 (2007) 3594-3600.
[73] D.L. Holliday, V. Speirs, Choosing the right cell line for breast cancer research, Breast Cancer Res, 13 (2011) 215.
[74] S. Domcke, R. Sinha, D.A. Levine, C. Sander, N. Schultz, Evaluating cell lines as tumour models by comparison of genomic profiles, Nat Commun, 4 (2013) 2126.
[75] N. Cancer Genome Atlas Research, J.N. Weinstein, E.A. Collisson, G.B. Mills, K.R. Shaw, B.A. Ozenberger, K. Ellrott, I. Shmulevich, C. Sander, J.M. Stuart, The Cancer Genome Atlas Pan-Cancer analysis project, Nat Genet, 45 (2013) 1113-1120.
[76] S. Carlsson, A.J. Vickers, M. Roobol, J. Eastham, P. Scardino, H. Lilja, J. Hugosson, Prostate cancer screening: facts, statistics, and interpretation in response to the US Preventive Services Task Force Review, J Clin Oncol, 30 (2012) 2581-2584.
[77] R. Edmondson, J.J. Broglie, A.F. Adcock, L. Yang, Three-dimensional cell culture systems and their applications in drug discovery and cell-based biosensors, Assay Drug Dev Technol, 12 (2014) 207-218.

[78] A. Birgersdotter, R. Sandberg, I. Ernberg, Gene expression perturbation in vitro--a growing case for three-dimensional (3D) culture systems, Semin Cancer Biol, 15 (2005) 405-412.
[79] K. Bhadriraju, C.S. Chen, Engineering cellular microenvironments to improve cell-based drug testing, Drug Discov Today, 7 (2002) 612-620.
[80] D. Motlagh, S.E. Senyo, T.A. Desai, B. Russell, Microtextured substrata alter gene expression, protein localization and the shape of cardiac myocytes, Biomaterials, 24 (2003) 2463-2476.
[81] L. Yin, H. Bien, E. Entcheva, Scaffold topography alters intracellular calcium dynamics in cultured cardiomyocyte networks, Am J Physiol Heart Circ Physiol, 287 (2004) H1276-1285.
[82] J. Kim, K.H. Chung, C.M. Lee, Y.S. Seo, H.C. Song, K.Y. Lee, Lymphatic delivery of 99mTc-labeled dextran acetate particles including cyclosporine A, J Microbiol Biotechnol, 18 (2008) 1599-1605.
[83] M.R. Junttila, F.J. de Sauvage, Influence of tumour micro-environment heterogeneity on therapeutic response, Nature, 501 (2013) 346-354.
[84] S.A. El-Hamid, A. Mogawer, In vitro mesenchymal stem cells differentiation into hepatocyte-like cells in the presence and absence of 3D microenvironment, Comparative Clinical Pathology, 23 (2014) 1051-1058.
[85] G.G. Giobbe, M. Zagallo, M. Riello, E. Serena, G. Masi, L. Barzon, B. Di Camillo, N. Elvassore, Confined 3D microenvironment regulates early differentiation in human pluripotent stem cells, Biotechnol Bioeng, 109 (2012) 3119-3132.
[86] M.C. Park, H. Jeong, S.H. Son, Y. Kim, D. Han, P.C. Goughnour, T. Kang, N.H. Kwon, H.E. Moon, S.H. Paek, D. Hwang, H.J. Seol, D.H. Nam, S. Kim, Novel Morphologic and Genetic Analysis of Cancer Cells in a 3D Microenvironment Identifies STAT3 as a Regulator of Tumor Permeability Barrier Function, Cancer Res, 76 (2016) 1044-1054.
[87] A.C. Luca, S. Mersch, R. Deenen, S. Schmidt, I. Messner, K.L. Schafer, S.E. Baldus, W. Huckenbeck, R.P. Piekorz, W.T. Knoefel, A. Krieg, N.H. Stoecklein, Impact of the 3D microenvironment on phenotype, gene expression, and EGFR inhibition of colorectal cancer cell lines, PLoS One, 8 (2013) e59689.
[88] K. Shield, M.L. Ackland, N. Ahmed, G.E. Rice, Multicellular spheroids in ovarian cancer metastases: Biology and pathology, Gynecol Oncol, 113 (2009) 143-148.
[89] J. Lee, M.J. Cuddihy, N.A. Kotov, Three-dimensional cell culture matrices: state of the art, Tissue Eng Part B Rev, 14 (2008) 61-86.
[90] K. Chitcholtan, P.H. Sykes, J.J. Evans, The resistance of intracellular mediators to doxorubicin and cisplatin are distinct in 3D and 2D endometrial cancer, J Transl Med, 10 (2012) 38.
[91] B. Fallica, J.S. Maffei, S. Villa, G. Makin, M. Zaman, Alteration of cellular behavior and response to PI3K pathway inhibition by culture in 3D collagen gels, PLoS One, 7 (2012) e48024.
[92] C. De Maria, S. Giusti, D. Mazzei, A. Crawford, A. Ahluwalia, Squeeze pressure bioreactor: a hydrodynamic bioreactor for noncontact stimulation of cartilage constructs, Tissue Eng Part C Methods, 17 (2011) 757-764.
[93] V. Hongisto, S. Jernstrom, V. Fey, J.P. Mpindi, K. Kleivi Sahlberg, O. Kallioniemi, M. Perala, High-throughput 3D screening reveals differences in drug sensitivities between culture models of JIMT1 breast cancer cells, PLoS One, 8 (2013) e77232.
[94] B.A. Justice, N.A. Badr, R.A. Felder, 3D cell culture opens new dimensions in cell-based assays, Drug Discov Today, 14 (2009) 102-107.

[95] T. Sun, S. Jackson, J.W. Haycock, S. MacNeil, Culture of skin cells in 3D rather than 2D improves their ability to survive exposure to cytotoxic agents, J Biotechnol, 122 (2006) 372-381.
[96] L.G. Griffith, M.A. Swartz, Capturing complex 3D tissue physiology in vitro, Nat Rev Mol Cell Biol, 7 (2006) 211-224.
[97] W.J. Ho, E.A. Pham, J.W. Kim, C.W. Ng, J.H. Kim, D.T. Kamei, B.M. Wu, Incorporation of multicellular spheroids into 3-D polymeric scaffolds provides an improved tumor model for screening anticancer drugs, Cancer Sci, 101 (2010) 2637-2643.
[98] A. Villasante, A. Marturano-Kruik, G. Vunjak-Novakovic, Bioengineered human tumor within a bone niche, Biomaterials, 35 (2014) 5785-5794.
[99] P. Koumoutsakos, I. Pivkin, F. Milde, The Fluid Mechanics of Cancer and Its Therapy, Annual Review of Fluid Mechanics, 45 (2013) 325-355.
[100] D.E. Jaalouk, J. Lammerding, Mechanotransduction gone awry, Nat Rev Mol Cell Biol, 10 (2009) 63-73.
[101] V. Vogel, M. Sheetz, Local force and geometry sensing regulate cell functions, Nat Rev Mol Cell Biol, 7 (2006) 265-275.
[102] A.C. Shieh, Biomechanical forces shape the tumor microenvironment, Ann Biomed Eng, 39 (2011) 1379-1389.
[103] M.A. Lancaster, J.A. Knoblich, Organogenesis in a dish: modeling development and disease using organoid technologies, Science, 345 (2014) 1247125.
[104] H. Clevers, Modeling Development and Disease with Organoids, Cell, 165 (2016) 1586-1597.
[105] X. Yin, B.E. Mead, H. Safaee, R. Langer, J.M. Karp, O. Levy, Engineering Stem Cell Organoids, Cell Stem Cell, 18 (2016) 25-38.
[106] T. Seino, S. Kawasaki, M. Shimokawa, H. Tamagawa, K. Toshimitsu, M. Fujii, Y. Ohta, M. Matano, K. Nanki, K. Kawasaki, S. Takahashi, S. Sugimoto, E. Iwasaki, J. Takagi, T. Itoi, M. Kitago, Y. Kitagawa, T. Kanai, T. Sato, Human Pancreatic Tumor Organoids Reveal Loss of Stem Cell Niche Factor Dependence during Disease Progression, Cell Stem Cell, 22 (2018) 454-467 e456.
[107] J. Drost, H. Clevers, Organoids in cancer research, Nature Reviews Cancer, 18 (2018) 407-418.
[108] D. Lee, D.N. Heo, S.J. Lee, M. Heo, J. Kim, S. Choi, H.-K. Park, Y.G. Park, H.-N. Lim, I.K. Kwon, Poly(lactide-co-glycolide) nanofibrous scaffolds chemically coated with gold-nanoparticles as osteoinductive agents for osteogenesis, Applied Surface Science, 432 (2018) 300-307.
[109] H. Amani, E. Mostafavi, H. Arzaghi, S. Davaran, A. Akbarzadeh, O. Akhavan, H. Pazoki-Toroudi, T.J. Webster, Three-Dimensional Graphene Foams: Synthesis, Properties, Biocompatibility, Biodegradability, and Applications in Tissue Engineering, ACS Biomaterials Science & Engineering, 5 (2019) 193-214.
[110] D.G. Castner, B.D. Ratner, Biomedical surface science: Foundations to frontiers, Surface Science, 500 (2002) 28-60.
[111] S. Breslin, L. O'Driscoll, Three-dimensional cell culture: the missing link in drug discovery, Drug Discov Today, 18 (2013) 240-249.
[112] P. Bradbury, B. Fabry, G.M. O'Neill, Occupy tissue, Cell Adhesion & Migration, 6 (2012) 424-520.

[113] B. Weigelt, C.M. Ghajar, M.J. Bissell, The need for complex 3D culture models to unravel novel pathways and identify accurate biomarkers in breast cancer, Adv Drug Deliv Rev, 69-70 (2014) 42-51.
[114] P. DelNero, Y.H. Song, C. Fischbach, Microengineered tumor models: insights & opportunities from a physical sciences-oncology perspective, Biomed Microdevices, 15 (2013) 583-593.
[115] C. Buchanan, M.N. Rylander, Microfluidic culture models to study the hydrodynamics of tumor progression and therapeutic response, Biotechnol Bioeng, 110 (2013) 2063-2072.
[116] C. Godugu, M. Singh, AlgiMatrix-Based 3D Cell Culture System as an In Vitro Tumor Model: An Important Tool in Cancer Research, Methods Mol Biol, 1379 (2016) 117-128.
[117] F.P. Seib, J.E. Berry, Y. Shiozawa, R.S. Taichman, D.L. Kaplan, Tissue engineering a surrogate niche for metastatic cancer cells, Biomaterials, 51 (2015) 313-319.
[118] S. Pradhan, I. Hassani, J.M. Clary, E.A. Lipke, Polymeric Biomaterials for In Vitro Cancer Tissue Engineering and Drug Testing Applications, Tissue Eng Part B Rev, 22 (2016) 470-484.
[119] X.H. Zhu, L.Y. Lee, J.S. Jackson, Y.W. Tong, C.H. Wang, Characterization of porous poly(D,L-lactic-co-glycolic acid) sponges fabricated by supercritical CO2 gas-foaming method as a scaffold for three-dimensional growth of Hep3B cells, Biotechnol Bioeng, 100 (2008) 998-1009.
[120] Z. Liu, G. Vunjak-Novakovic, Modeling tumor microenvironments using custom-designed biomaterial scaffolds, Current Opinion in Chemical Engineering, 11 (2016) 94-105.
[121] A.E. Guller, P.N. Grebenyuk, A.B. Shekhter, A.V. Zvyagin, S.M. Deyev, Bioreactor-Based Tumor Tissue Engineering, Acta Naturae, 8 (2016) 44-58.
[122] S. Bauer, P. Schmuki, K. von der Mark, J. Park, Engineering biocompatible implant surfaces: Part I: Materials and surfaces, Progress in Materials Science, 58 (2013) 261-326.
[123] A.A. Khalili, M.R. Ahmad, A Review of Cell Adhesion Studies for Biomedical and Biological Applications, Int J Mol Sci, 16 (2015) 18149-18184.
[124] V. Montano-Machado, P. Chevallier, D. Mantovani, E. Pauthe, On the potential for fibronectin/phosphorylcholine coatings on PTFE substrates to jointly modulate endothelial cell adhesion and hemocompatibility properties, Biomatter, 5 (2015) e979679.
[125] R. Agarwal, C. Gonzalez-Garcia, B. Torstrick, R.E. Guldberg, M. Salmeron-Sanchez, A.J. Garcia, Simple coating with fibronectin fragment enhances stainless steel screw osseointegration in healthy and osteoporotic rats, Biomaterials, 63 (2015) 137-145.
[126] S. Chen, C.Y. Lee, R.W. Li, P.N. Smith, Q.H. Qin, Modelling osteoblast adhesion on surface-engineered biomaterials: optimisation of nanophase grain size, Computer Methods in Biomechanics and Biomedical Engineering, 20 (2017) 905-914.
[127] X. Guan, Cancer metastases: challenges and opportunities, Acta Pharm Sin B, 5 (2015) 402-418.
[128] A.M. Alizadeh, S. Shiri, S. Farsinejad, Metastasis review: from bench to bedside, Tumour Biol, 35 (2014) 8483-8523.
[129] A. Fuhrmann, A. Banisadr, P. Beri, T.D. Tlsty, A.J. Engler, Metastatic State of Cancer Cells May Be Indicated by Adhesion Strength, Biophys J, 112 (2017) 736-745.
[130] S. Stratton, N.B. Shelke, K. Hoshino, S. Rudraiah, S.G. Kumbar, Bioactive polymeric scaffolds for tissue engineering, Bioact Mater, 1 (2016) 93-108.
[131] D.M. Li, Y.M. Feng, Signaling mechanism of cell adhesion molecules in breast cancer metastasis: potential therapeutic targets, Breast Cancer Res Treat, 128 (2011) 7-21.

[132] C. Fischbach, R. Chen, T. Matsumoto, T. Schmelzle, J.S. Brugge, P.J. Polverini, D.J. Mooney, Engineering tumors with 3D scaffolds, Nat Methods, 4 (2007) 855-860.
[133] S.P. Pathi, C. Kowalczewski, R. Tadipatri, C. Fischbach, A novel 3-D mineralized tumor model to study breast cancer bone metastasis, PLoS One, 5 (2010) e8849.
[134] E.L. Fong, S.E. Lamhamedi-Cherradi, E. Burdett, V. Ramamoorthy, A.J. Lazar, F.K. Kasper, M.C. Farach-Carson, D. Vishwamitra, E.G. Demicco, B.A. Menegaz, H.M. Amin, A.G. Mikos, J.A. Ludwig, Modeling Ewing sarcoma tumors in vitro with 3D scaffolds, Proc Natl Acad Sci U S A, 110 (2013) 6500-6505.
[135] X. Li, Y. Chen, P.C. Li, A simple and fast microfluidic approach of same-single-cell analysis (SASCA) for the study of multidrug resistance modulation in cancer cells, Lab Chip, 11 (2011) 1378-1384.
[136] G. Velve-Casquillas, M. Le Berre, M. Piel, P.T. Tran, Microfluidic tools for cell biological research, Nano Today, 5 (2010) 28-47.
[137] J.H. Sung, M.L. Shuler, A micro cell culture analog (microCCA) with 3-D hydrogel culture of multiple cell lines to assess metabolism-dependent cytotoxicity of anti-cancer drugs, Lab Chip, 9 (2009) 1385-1394.
[138] J. Autebert, B. Coudert, F.C. Bidard, J.Y. Pierga, S. Descroix, L. Malaquin, J.L. Viovy, Microfluidic: an innovative tool for efficient cell sorting, Methods, 57 (2012) 297-307.
[139] A.M. Ghaemmaghami, M.J. Hancock, H. Harrington, H. Kaji, A. Khademhosseini, Biomimetic tissues on a chip for drug discovery, Drug Discov Today, 17 (2012) 173-181.
[140] J.L. Carvalho, P.H.d. Carvalho, D.A. Gomes, A.d.M. Góes, Innovative Strategies for Tissue Engineering, 2013.
[141] A. Ravichandran, Y. Liu, S.H. Teoh, Review: bioreactor design towards generation of relevant engineered tissues: focus on clinical translation, J Tissue Eng Regen Med, 12 (2018) e7-e22.
[142] A.R. Amini, C.T. Laurencin, S.P. Nukavarapu, Bone tissue engineering: recent advances and challenges, Crit Rev Biomed Eng, 40 (2012) 363-408.
[143] B.V. Slaughter, S.S. Khurshid, O.Z. Fisher, A. Khademhosseini, N.A. Peppas, Hydrogels in regenerative medicine, Adv Mater, 21 (2009) 3307-3329.
[144] B. Altmann, A. Welle, S. Giselbrecht, R. Truckenmuller, E. Gottwald, The famous versus the inconvenient - or the dawn and the rise of 3D-culture systems, World J Stem Cells, 1 (2009) 43-48.
[145] L. Ma, J. Barker, C. Zhou, W. Li, J. Zhang, B. Lin, G. Foltz, J. Kublbeck, P. Honkakoski, Towards personalized medicine with a three-dimensional micro-scale perfusion-based two-chamber tissue model system, Biomaterials, 33 (2012) 4353-4361.
[146] M.J. Bissell, D. Radisky, Putting tumours in context, Nat Rev Cancer, 1 (2001) 46-54.
[147] G. Christofori, H. Semb, The role of the cell-adhesion molecule E-cadherin as a tumour-suppressor gene, Trends Biochem Sci, 24 (1999) 73-76.
[148] A. Lochter, S. Galosy, J. Muschler, N. Freedman, Z. Werb, M.J. Bissell, Matrix metalloproteinase stromelysin-1 triggers a cascade of molecular alterations that leads to stable epithelial-to-mesenchymal conversion and a premalignant phenotype in mammary epithelial cells, J Cell Biol, 139 (1997) 1861-1872.
[149] I.K. Zervantonakis, S.K. Hughes-Alford, J.L. Charest, J.S. Condeelis, F.B. Gertler, R.D. Kamm, Three-dimensional microfluidic model for tumor cell intravasation and endothelial barrier function, Proc Natl Acad Sci U S A, 109 (2012) 13515-13520.

[150] A.L. Paguirigan, D.J. Beebe, From the cellular perspective: exploring differences in the cellular baseline in macroscale and microfluidic cultures, Integr Biol (Camb), 1 (2009) 182-195.
[151] V.I. Sikavitsas, G.N. Bancroft, H.L. Holtorf, J.A. Jansen, A.G. Mikos, Mineralized matrix deposition by marrow stromal osteoblasts in 3D perfusion culture increases with increasing fluid shear forces, Proc Natl Acad Sci U S A, 100 (2003) 14683-14688.
[152] M.A. Woodruff, C. Lange, F. Chen, P. Fratzl, D.W. Hutmacher, Nano- to macroscale remodeling of functional tissue-engineered bone, Adv Healthc Mater, 2 (2013) 546-551.
[153] W.L. Grayson, D. Marolt, S. Bhumiratana, M. Frohlich, X.E. Guo, G. Vunjak-Novakovic, Optimizing the medium perfusion rate in bone tissue engineering bioreactors, Biotechnol Bioeng, 108 (2011) 1159-1170.
[154] R.A. Thibault, A.G. Mikos, F.K. Kasper, Scaffold/Extracellular matrix hybrid constructs for bone-tissue engineering, Adv Healthc Mater, 2 (2013) 13-24.
[155] C. Hirt, A. Papadimitropoulos, M.G. Muraro, V. Mele, E. Panopoulos, E. Cremonesi, R. Ivanek, E. Schultz-Thater, R.A. Droeser, C. Mengus, M. Heberer, D. Oertli, G. Iezzi, P. Zajac, S. Eppenberger-Castori, L. Tornillo, L. Terracciano, I. Martin, G.C. Spagnoli, Bioreactor-engineered cancer tissue-like structures mimic phenotypes, gene expression profiles and drug resistance patterns observed "in vivo", Biomaterials, 62 (2015) 138-146.
[156] L.E. Marshall, K.F. Goliwas, L.M. Miller, A.D. Penman, A.R. Frost, J.L. Berry, Flow-perfusion bioreactor system for engineered breast cancer surrogates to be used in preclinical testing, J Tissue Eng Regen Med, 11 (2017) 1242-1250.
[157] L.K. Chim, A.G. Mikos, Biomechanical forces in tissue engineered tumor models, Current Opinion in Biomedical Engineering, 6 (2018) 42-50.
[158] M. Santoro, S.E. Lamhamedi-Cherradi, B.A. Menegaz, J.A. Ludwig, A.G. Mikos, Flow perfusion effects on three-dimensional culture and drug sensitivity of Ewing sarcoma, Proc Natl Acad Sci U S A, 112 (2015) 10304-10309.
[159] J.F. Alvarez-Barreto, B. Landy, S. VanGordon, L. Place, P.L. DeAngelis, V.I. Sikavitsas, Enhanced osteoblastic differentiation of mesenchymal stem cells seeded in RGD-functionalized PLLA scaffolds and cultured in a flow perfusion bioreactor, J Tissue Eng Regen Med, 5 (2011) 464-475.
[160] J.F. Alvarez-Barreto, V.I. Sikavitsas, Improved mesenchymal stem cell seeding on RGD-modified poly(L-lactic acid) scaffolds using flow perfusion, Macromol Biosci, 7 (2007) 579-588.
[161] M.R. Vieyra-Lobato, J. Vela-Ojeda, L. Montiel-Cervantes, R. López-Santiago, M.C. Moreno-Lafont, Description of CD8(+) Regulatory T Lymphocytes and Their Specific Intervention in Graft-versus-Host and Infectious Diseases, Autoimmunity, and Cancer, Journal of immunology research, 2018 (2018) 3758713.
[162] L.J. Taite, M.L. Rowland, K.A. Ruffino, B.R. Smith, M.B. Lawrence, J.L. West, Bioactive hydrogel substrates: probing leukocyte receptor-ligand interactions in parallel plate flow chamber studies, Ann Biomed Eng, 34 (2006) 1705-1711.
[163] G.L. Szeto, D. Van Egeren, H. Worku, A. Sharei, B. Alejandro, C. Park, K. Frew, M. Brefo, S. Mao, M. Heimann, R. Langer, K. Jensen, D.J. Irvine, Microfluidic squeezing for intracellular antigen loading in polyclonal B-cells as cellular vaccines, Scientific reports, 5 (2015) 10276-10276.
[164] E.R. Sauter, Exosomes in blood and cancer, Translational Cancer Research, (2017) S1316-S1320.

[165] Y. Ning, K. Shen, Q. Wu, X. Sun, Y. Bai, Y. Xie, J. Pan, C. Qi, Tumor exosomes block dendritic cells maturation to decrease the T cell immune response, Immunol Lett, 199 (2018) 36-43.
[166] M.N. Theodoraki, S.S. Yerneni, T.K. Hoffmann, W.E. Gooding, T.L. Whiteside, Clinical Significance of PD-L1(+) Exosomes in Plasma of Head and Neck Cancer Patients, Clin Cancer Res, 24 (2018) 896-905.
[167] P. Sharma, B. Diergaarde, S. Ferrone, J.M. Kirkwood, T.L. Whiteside, Melanoma cell-derived exosomes in plasma of melanoma patients suppress functions of immune effector cells, Scientific Reports, 10 (2020) 92.

7. SUPPLEMENTARY MATERIAL

7.1 Calibration Curves

7.1.1 Poly K Calibration

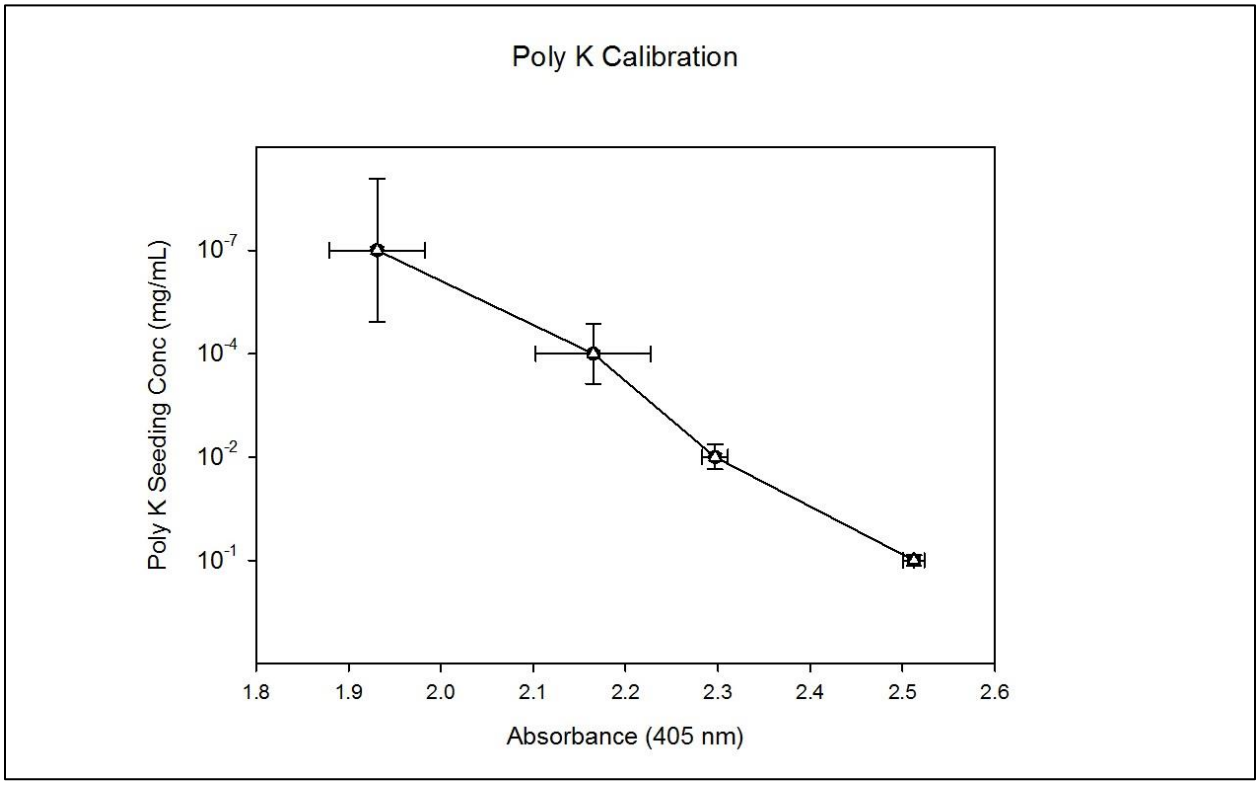

Figure 16: **Calibration curve for poly K detection using concentrations from 0.1 mg/mL to 0.0000001 mg/mL**

Figure 16 illustrates the calibration curve used for poly K detection. 1 mL of known concentrations of poly K ranging from 10-1 mg/mL to 10-7 mg/mL were placed into a 48 well plate and reacted with HRP to obtain absorbance readings. A standard curve was generated as $y = -10.605x + 27.111$ with an R^2 value of 0.9521.

7.1.2 RGD Calibration

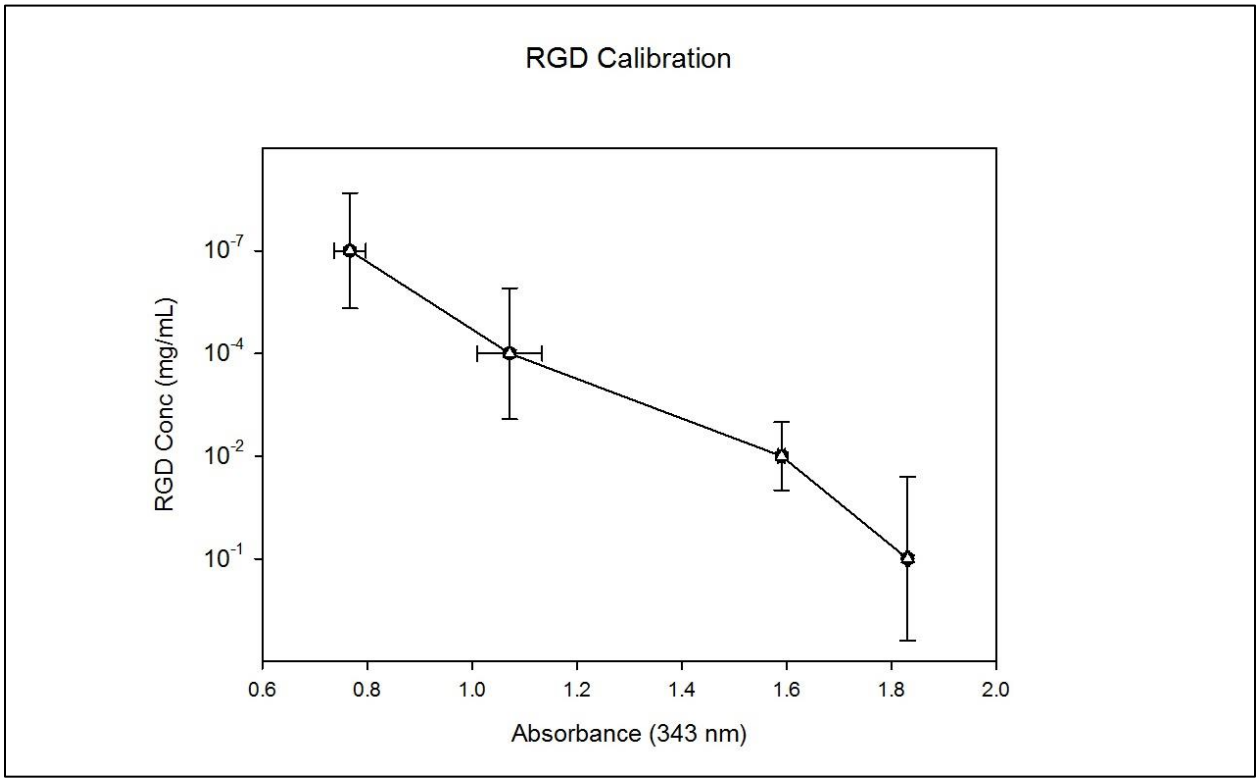

Figure 17**: Calibration curve for RGD detection using concentrations of RGD ranging from 0.1 mg/mL to 0.0000001 mg/mL alongside corresponding SPDP concentrations.**

Figure 17 illustrates the calibration curve for RGD detection. Mole breakdown could be done based on the surface modification chemistry provided in Figure 2. Equal concentrations of RGDC and SPDP were reacted in a 48 well plate for a total volume of 1 mL. The reaction was then read under a plate reader at 343 nm and generated a standard curve of $y = -5.3339x + 10.513$ with an R^2 value of 0.9508.

7.1.3 T-Cell Calibration

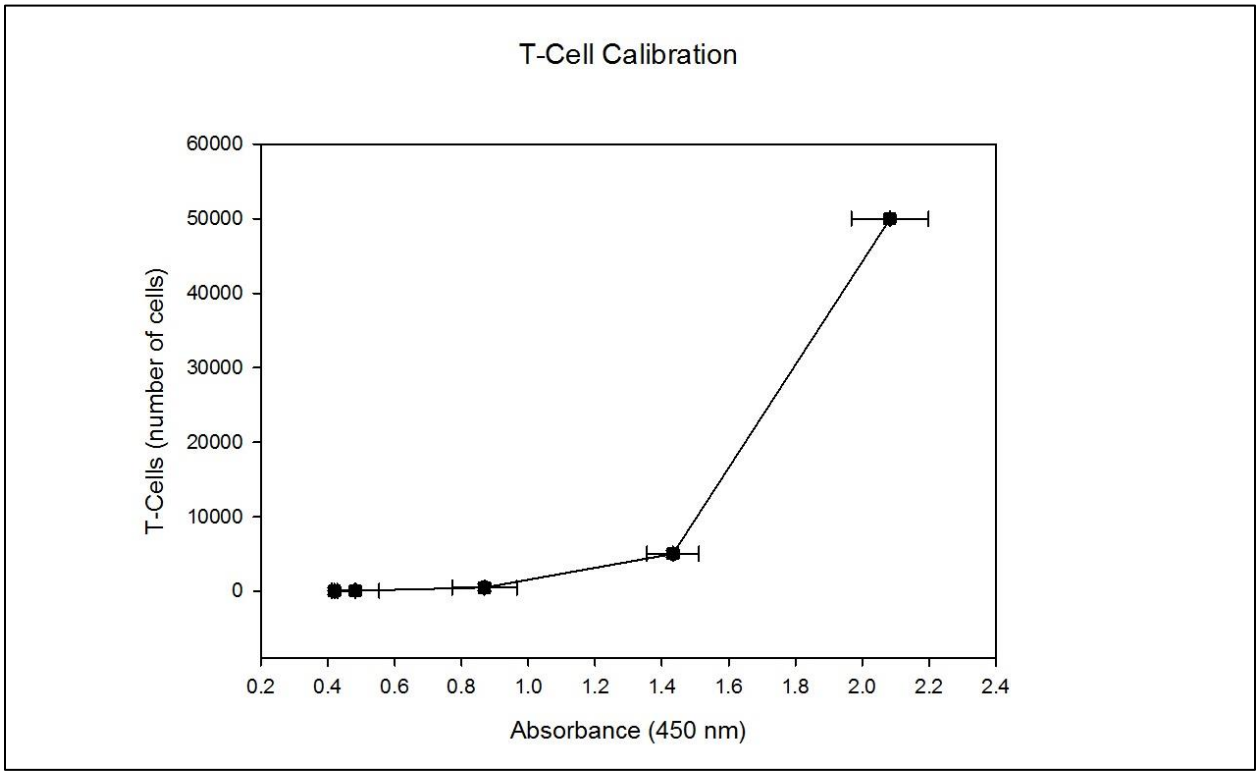

Figure 18: **Calibration curve for T-cell quantification using T-cell numbers ranging from magnitudes of 50,000 to 5.**

Figure 18 illustrates the calibration curve for T-cell quantification using PMA stimulation detection of IL-2 production. As said above, flow cytometry was used to ascertain the number of T-cells in each well. Each well was stimulated with 10 µM PMA for 4 hours. As per the ELISA instructions, samples were taken, processed, and read in a plater reader at a 450 nm wavelength to generate an absorbance graph. The standard curve generated was $y = 0.0972x^2 - 0.0944x + 0.4507$ and a R^2 value of 0.9975. A lag in the curve was expected due to the relatively high concentration of PMA which overstimulates lower concentration of T-cells which lags IL-2 production.

7.1.4 IL-2 Calibration

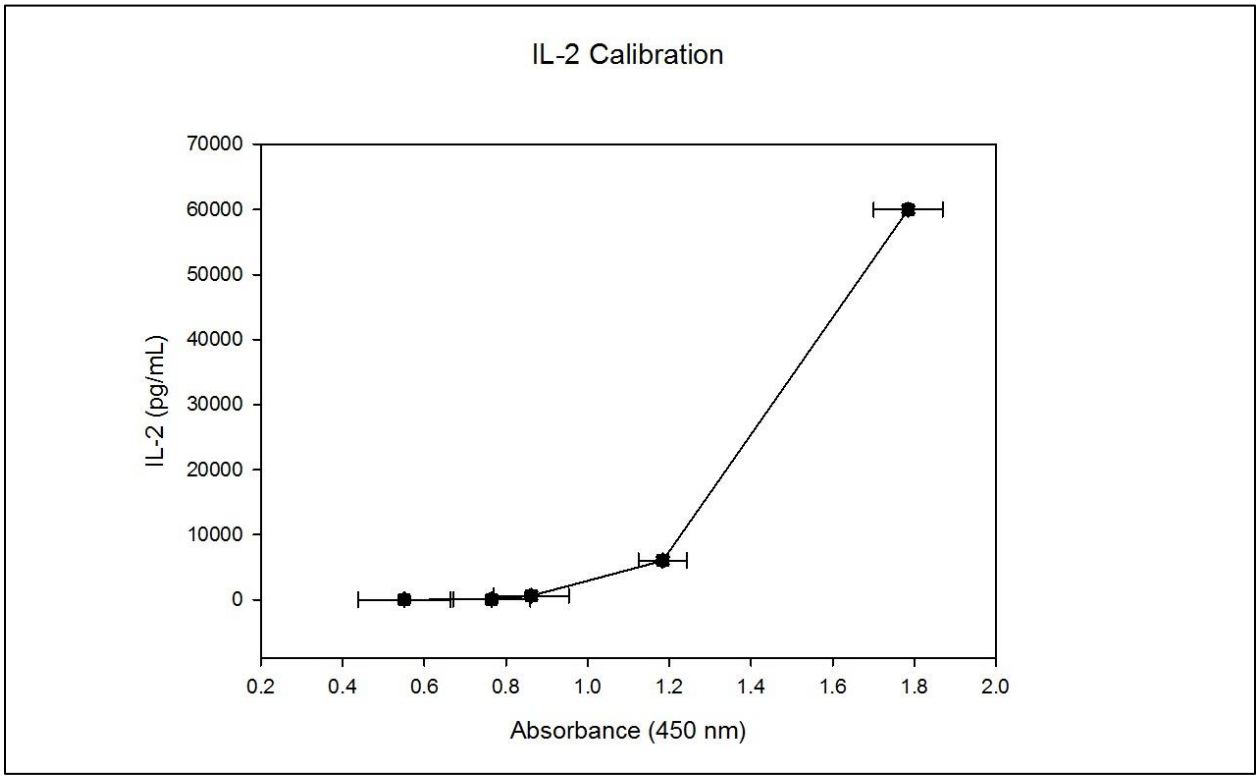

Figure 19**: Calibration curve for IL-2 detection with concentrations rangng from 60,000 pg/mL to 6 pg/mL.**

Figure 19 illustrates the calibration curve for IL-2 quantification based on provided IL-2 dilutions in the IL-2 ELISA detection kit. IL-2 standards were generated from 60,000 pg/mL of standard to 6 pg/mL. Standards were prepared alongside samples for IL-2 detection and read in a plate reader at a 450 nm wavelength. The standard curve generated was $y = 43692x^3 - 88747x^2 + 60495x - 13714$ with an R2 value of 0.9715.

7.1.5 RGD Dose Response

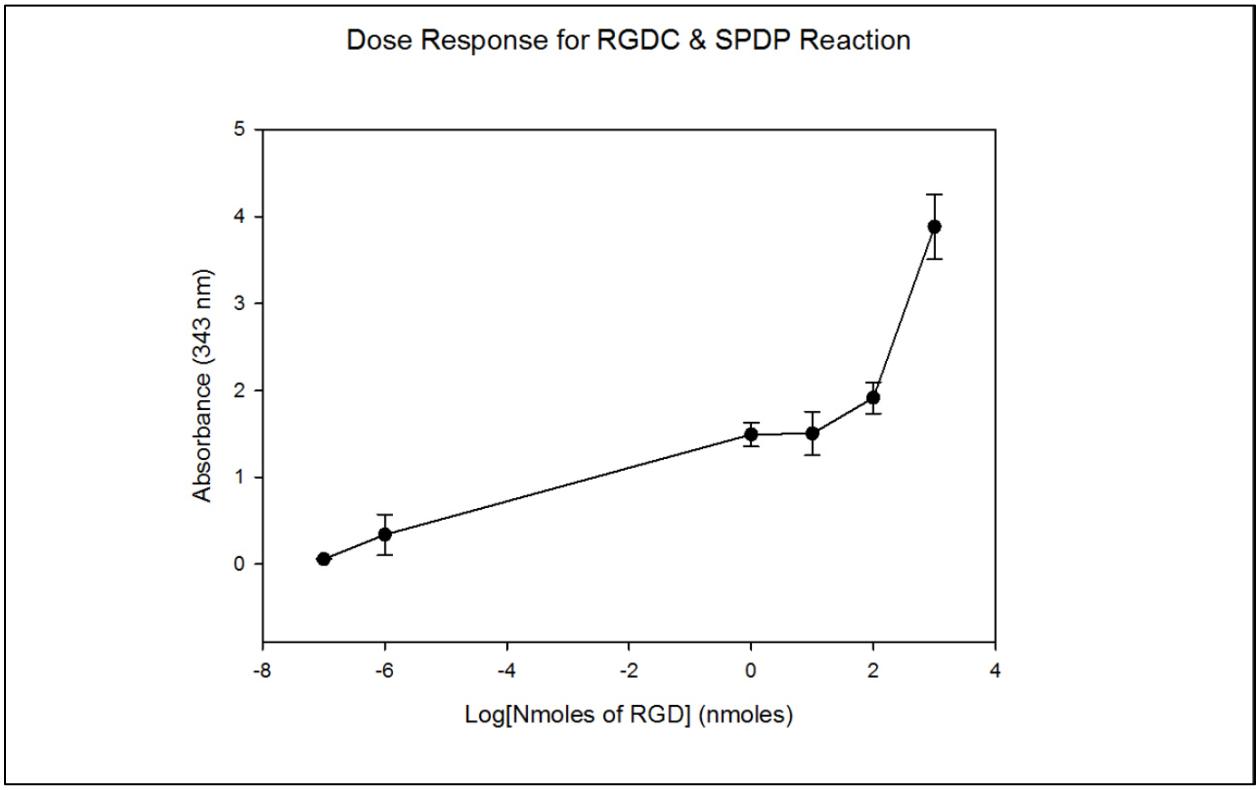

Figure 20**: RGDC & SPDP reaction dose response ranging from 10^{-7} nmoles to 1000 nmoles.**

Figure 20 illustrates the dose response for RGD reacted with SPDP based on increasing nmoles of RGDC. Standards were generated by reacting known concentrations and nmoles of both RGDC and SPDP to generate a dose response. Standards were prepared alongside samples for surface modification and read in a plate reader at a 343 nm wavelength. The standard curve generated was $y = 0.00152x^5 + 0.0182x^4 + 0.0457x^3 - 0.0867x^2 + 0.0323x - 1.4926$ with an R2 value of 0.9884.